Permanent Magnet Synchronous Machine Vibration Measurement System

by

Diego Fernández Laborda

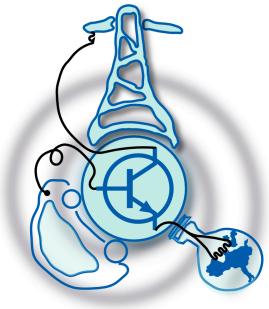

Submitted to the Department of Electrical Engineering, Electronics, Computers and Systems
in partial fulfillment of the requirements for the degree of
Master of Science in Electrical Energy Conversion and Power Systems
at the
UNIVERSIDAD DE OVIEDO
July 2018

Author .....

Certified by .....
David Díaz Reigosa
Associate Professor
Thesis Supervisor

Certified by .....
Daniel Fernández Alonso
Assistant Professor
Thesis Supervisor

Permanent Magnet Synchronous Machine Vibration Measurement System

by

Diego Fernández Laborda

Submitted to the Department of Electrical Engineering, Electronics, Computers and Systems
on July 24, 2018, in partial fulfillment of the
requirements for the degree of
Master of Science in Electrical Energy Conversion and Power Systems

Abstract

Permanent Magnet Synchronous Motors (PMSMs) have been massively introduced in the industry in the recent years due to its better characteristics compared to other machines but they have higher torque ripple and vibrations. Those vibrations sometimes are not compatible with their application such as lifts, escalators and robotics. Additionally, the interest in Fault Detection Diagnosis (FDD) techniques for PMSMs have increased since its introduction in the industry. In this master thesis, a vibration measurement system able to detect faults in a PMSM and to suppress machine vibrations is developed. The FDD capability of the prototype is tested through experimental results by creating magnetization faults in an Interior PMSM (IPMSM). Finally, a new vibration suppression control scheme is proposed and simulated showing the cancellation of several torque ripple harmonics.

Thesis Supervisor: David Díaz Reigosa
Title: Associate Professor

Thesis Supervisor: Daniel Fernández Alonso
Title: Assistant Professor

Acknowledgments

Me gustaría agradecer a mi tutor David Díaz Reigosa y mi co-tutor Daniel Fernández Alonso por todo el apoyo que me habéis ofrecido durante la realización de mi tesis. Gracias por toda la ayuda, conocimientos y experiencia que me habéis transmitido, pero sobretodo por escuchar e incentivar el desarrollo de mis ideas.

También me gustaría agradecer la ayuda económica recibida a Thyssenkrupp que ha financiado íntegramente este proyecto mediante la adjudicación de la ayuda para la realización de Trabajos Fin de Máster en el marco de la Cátedra de Movilidad financiada por Thyssenkrupp.

Gracias María y Cristina por tantísimas horas que habéis sacado de vuestro tiempo para ayudarme y por vuestra simpatía, que en este corto periodo de tiempo que llevo trabajando a vuestro lado, me ha hecho sentir como en casa.

No quiero olvidarme de agradecer a mis compañeros de máster su cariño y compañia durante esta aventura de dos años que este TFM pone fin. La verdad que dos años parece poco tiempo comparado con todo lo que hemos vivido juntos y el aprecio que os he cogido desde que os conocí, unos el primer día de máster, y otros hace bastante más tiempo. Gracias sobretodo a ti, Migui, que tantas largas noches hemos pasado "juntos" en llamada hasta altas horas de la madrugada haciendo el trabajo de turno.

Muchisimas gracias a ti, Rosana, que podría redactar cien tesis enteras sólo para agradecerte todo lo que te debo. Gracias por estar a mi lado siempre sin importar mi humor, gracias por sacarme mil sonrisas cada día, por motivarme a seguir adelante y por hacerme mejor persona. Gracias a ti y a tu familia.

Por último, pero no menos importante, agradecer a mis padres su apoyo incondicional y por ayudarme a mantener siempre los pies en la tierra. Espero que estéis orgullosos de mí y siempre daré el máximo para que así os sintáis, vosotros y toda mi familia.

Contents

List of Figures

List of Tables

Chapter 1

Introduction

In recent years, Permanent Magnet Synchronous Motors (PMSMs) have been massively introduced in the Industry in different applications (electric or hybrid vehicles, railway traction, lifts, wind generation, aeronautics, aerospace and naval) due to its better characteristics compared to other types of electric machines such as Induction Machines (IMs) or DC Machines. PMSMs exhibits a better efficiency, power density and controllability, but they have higher torque ripple, risk of demagnetization and higher cost due to the rare-earth magnets.

The integration of this kind of machines in the industry has increased the interest in several research topics, the most common ones are: contributions to increase the performance of PMSMs, studies of efficiency and losses, torque ripple minimization, parameters estimation and sensorless control, flux calculation and models, diagnosis, variable flux machines and multiphase machines.

In the industry, the interest in the development of Fault Detection Diagnosis (FDD) techniques in PMSMs has increased because they help prevent unexpected downtimes and optimise maintenance. The most used FDD techniques are based on: magnetic field monitoring, temperature monitoring, RF emissions monitoring, vibration and noise monitoring, Motor Current Signature Analysis (MCSA) and techniques based in neural networks and artificial intelligence [1]. However, some of these techniques are not mature enough for their use in the industry.

Among the previously described techniques, vibration analysis and monitoring is

one of the most extended predictive maintenance techniques and FDD in the industry. Nevertheless, there are intrinsic vibrations in PMSMs in normal operation due to constructive aspects (relation between number of rotor poles and stator slots, stator slots design, design and number of flux barriers in the rotor...) and constructive tolerances of the machine (rotor eccentricity, tolerances in the bearings...). Sometimes, these vibrations are not allowed by the load or application and, furthermore, they contribute to the premature failure of other elements such as the bearings, which are the most frequent kind of faults in electric machines [2]. Both vibrations due to faults and vibrations due to constructive aspects and tolerances of the machine can be detected by vibration monitoring. Additionally, the information from a vibration monitoring system can be used for both FDD and control feedback of the machine to develop an active vibration reduction system and decrease the fatigue failure rate.

In order to make such feedback, a control scheme must be proposed and a vibration sensor needs to be developed. It has been demonstrated in [3] that it is possible to cancel vibrations and torque ripple harmonics subtracting those harmonics from the desired torque command with a feedforward control scheme.

The aim of this thesis is to design a vibration monitoring system attachable to the stator of the machine which can be used for FDD and vibration control of PMSMs. Furthermore, it is of a great interest to make a comparison of this vibration measurement system with previously developed systems.

Chapter 2

Objectives of the Master Thesis

The industrial and research interest in PMSMs has been stated in Chapter 1. This master thesis is meant to contribute in the topics of torque ripple minimization, vibration control and diagnosis. The main objective is the design and manufacture of a vibration monitoring system which can be easily attach to the stator of the machine. This prototype will allow to:

- Develop a Fault Detection Diagnosis system able to identify faults in a PMSM based in the spectral harmonic content of vibration measurements.
- Propose a control scheme in order to minimise vibrations in the machine, which increases the lifetime of the machine and allows it to work under some fault conditions.
- Make a comparison between this vibration measurement system and previous developed ones.

Chapter 3

State of the Art

In PMSMs there are several sources of vibration: usual vibrations due to the torque ripple, constructive aspects, tolerances in the manufacturing process of the machine and vibrations due to faults. In this chapter a review of the different sources of vibration in PMSMs, the frequency components that are related to faults and other existing diagnosis methods is performed and finally the previous work in vibration control is analysed.

3.1 Constructive Aspects

Constructive aspects of PMSMs such as number of slots, number of poles and flux barriers in the rotor create intrinsic vibrations during normal operation of the machine.

The teeth and slots make small variations in the airgap reluctance and, therefore, change the radial and axial flux. In the existing literature, vibrations are related with the radial flux in the airgap by means of the Maxwell stress tensor [4][5][6]. The vibration frequency related with this phenomenom is the product of slot number and the mechanical speed of the machine [7]. These vibrations can be reduced with a proper motor design by skewing the stator slots.

The flux barriers are used in order to reduce the rotor magnet leakage flux, increasing the rotor reluctance path and forcing the magnet flux to flow through the

stator. The shape, number and location of those flux barriers affect the airgap flux and its distribution.

The pole and slot number combination has a great influence in the vibration and noise produced by the motor. Among the produced vibrations by this constructive aspect, the Cogging Torque and its reduction is one of the most researched ones and a lot of effort has been made in that subject.

3.2 Tolerances

In the manufacturing process of the machine, the stator and rotor shape is not perfect due to usual fabrication tolerances. This fact makes that two machines manufactured in the same production line have different vibration shapes and magnitudes. Some literature has been made in the study of the effects that manufacturing tolerances and asymmetries have in the machine behaviour. In [8], variations due to tolerances such as slot opening variations, radial and tangential asymmetry and eccentricity are studied.

3.3 Torque Ripple

Other important source of vibrations is the torque ripple of the machine. Torque ripple is a periodic torque fluctuation which does not contribute to the average torque or speed, thus not producing useful power. These periodic torque fluctuations are transferred from the rotor to the stator of the machine by Newton's third law, producing stator vibrations.

There are three sources of torque ripple: reluctance torque, cogging torque and mutual torque ripple [9]. This can be seen in the synchronous reference frame torque equation (3.1), where the first term is the mutual torque contribution, the second term is the reluctance torque contribution and the third term is the cogging torque.

$$T = \frac{2 \cdot p}{3}\left[\varphi_m \cdot I_q + (L_d - L_q) \cdot I_d \cdot I_q\right] + T_{cog} \tag{3.1}$$

3.3.1 Reluctance Torque

The reluctance torque is caused by the variation of the stator inductances with rotor position. This variation is usually called saliency, which is used in some sensorless methods to estimate the rotor position [10].

In Interior Permanent Magnet Synchronous Motors (IPMSMs), the synchronous reference frame "d-axis" is aligned with the rotor flux created by the magnets. This alignment makes the "d-axis" inductance lower than the "q-axis" inductance due to the presence of the magnets which increase the reluctance path. In this reference frame, the stator inductances have only small variations with rotor position (due to constructive aspects: stator slots; or tolerances: rotor eccentricity) because the largest contribution is the magnet size, therefore it is safe to assume constant inductances in this reference frame. From this assumption, it is easy to realise that for negative values of I_d in equation (3.1) the average value of the torque is increased. This fact has lead into multiple strategies, which minimize the copper losses for a given desired torque, called Maximum Torque Per Ampere (MTPA) strategies [11].

3.3.2 Cogging Torque

The Cogging Torque is produced by the interaction of the flux created by the rotor magnets with the stator slots. Despite the other torque ripples, Cogging Torque has no dependence in stator currents, and therefore it can not be detected through current measurements. But all torque ripples can be detected through mechanical sensors [3].

As it has been stated before, a lot of effort has been made in order to minimize the Cogging Torque in PMSMs for high precision applications. In the literature, there are several Cogging Torque reduction techniques such as rotor or stator skewing, increasing the number of phases, maximization of the least common multiple (LCM) of pole and slot number and harmonic current injection [12][13][14]. In [6], it is shown that contribution to vibrations of the asymmetrical winding pattern , used in some machine configurations (8-pole/9-slot) to reduce the Cogging Torque, is significant. Therefore, increasing the slot-pole LCM does not necessary reduce the total vibrations

of the machine.

3.3.3 Mutual torque ripple

The mutual torque ripple is produced by the interaction of three-phase currents and airgap flux, being one or both of them not perfectly sinusoidal. Theoretically, the airgap flux created by the magnets following a sinusoidal space distribution will generate sinusoidal Back-EMF voltages in the stator windings, but, in reality, the flux created by the rotor magnets it is not completely sinusoidal and it generates Back-EMF harmonics, torque ripple and vibrations. To counteract this effect, some current injection techniques have been developed, proving that non sinusoidal currents can be used to reduce torque ripple [15].

One of the reasons for the existence of harmonics in the airgap flux are the variations in the reluctance path due to stator slots. This reluctance variation decreases the inductance when a stator slot appears in the flux path and, therefore, the airgap flux density is decreased [16]. In order to add the possibility to account for such variations in the flux density and inductances, a model in synchronous reference frame is developed taking into account those variations.

Machine model for non-constant inductances

The model of a PMSM in the rotor synchronous reference frame with no rotor cage is shown in equation (3.2) [17], where R_s is the stator resistance, i_{dq} is the stator current, λdqs is the stator flux linkage, w_r is the rotor angular speed, L_{dqs} is the stator inductance and λ_{PM} is the magnet flux linkage.

$$\begin{aligned} v_d &= R_s i_d + \frac{d}{dt}\lambda_{ds} - w_r \lambda_{qs} \\ v_q &= R_s i_q + \frac{d}{dt}\lambda_{qs} + w_r \lambda_{ds} \\ \lambda_{ds} &= L_{ds} i_d + \lambda_{PM} \\ \lambda_{qs} &= L_{qs} i_q \end{aligned} \tag{3.2}$$

Usually we assume constant permanent magnet flux and constant inductances,

getting the commonly used model shown in equation (3.3).

$$\begin{aligned} v_d &= R_s i_d + L_{ds}\frac{d}{dt}i_d - w_r L_{qs} i_q \\ v_q &= R_s i_q + L_{qs}\frac{d}{dt}i_q + w_r L_{ds} i_d + w_r \lambda_{PM} \end{aligned} \tag{3.3}$$

In order to expand the model to take into account the inductance variations and consequently the flux variations, the time derivative of the flux in the rotor synchronous reference frame is calculated in equation (3.4), where L_{mds} is the direct axis mutual inductance and I_f is the magnetizing current of the magnet, which is a measure of its magnetization.

$$\begin{aligned} \frac{d}{dt}\lambda_{ds} &= L_{ds}\frac{d}{dt}i_d + i_d\frac{d}{dt}L_{ds} + L_{mds}\frac{d}{dt}I_f + I_f\frac{d}{dt}L_{mds} \\ \frac{d}{dt}\lambda_{qs} &= L_{qs}\frac{d}{dt}i_q + i_q\frac{d}{dt}L_{qs} \end{aligned} \tag{3.4}$$

The term $L_{ds}\frac{d}{dt}i_d$ is used to calculate the direct axis phase current with the differential equation. The term $L_{mds}\frac{d}{dt}I_f$ stands for the variation of the magnet magnetization which for a PMSM must be zero but for a Variable-Flux machine can be important during magnetization and magnetization process. The terms $i_d\frac{d}{dt}L_{ds}$ and $I_f\frac{d}{dt}L_{mds}$ are meant to account for the inductance-time variation. Knowing the fact that the stator direct axis inductance is the sum of the leakage and the mutual direct axis inductances, and assuming constant leakage inductance L_{lds} , the relation in equation (3.5) is given.

$$\frac{d}{dt}L_{ds} = \frac{d}{dt}\big(L_{mds} + L_{lds}\big) = \frac{d}{dt}L_{mds} \tag{3.5}$$

As it is said before, the inductance variation is caused by the reluctance path variation, but the reluctance path is a space dependant variable which will be higher when the flux path goes through a stator slot and lower when the flux path goes directly to the stator teeth. In equations (3.4) and (3.5), the relation between flux time-derivative and mutual inductance time-derivative is stated, but it has much more sense to relate the mutual inductance to a space variable such as the rotor angle θ. Therefore, the relation between the time-derivative of the mutual inductance and its

angle-derivative is calculated in equation (3.6).

$$\frac{d}{dt}L_{mds} = \frac{d\theta}{dt}\frac{d}{d\theta}L_{mds} = w_r\frac{d}{d\theta}L_{mds} \tag{3.6}$$

Using equations (3.6), (3.5), (3.4) and substituting into (3.2) and rearranging terms, the PMSM model for variable inductances is shown in equation (3.7)

$$\begin{aligned} v_d &= R_s i_d + L_{ds}\frac{d}{dt}i_d + w_r(i_d + I_f)\frac{d}{d\theta}L_{mds} - w_r L_{qs} i_q \\ v_q &= R_s i_q + L_{qs}\frac{d}{dt}i_q + w_r i_q \frac{d}{d\theta}L_{mqs} + w_r L_{ds} i_d + w_r \lambda_{PM} \end{aligned} \tag{3.7}$$

3.4 Vibration Monitoring Diagnosis

The usual PMSMs faults can be classified into electric, magnetic and mechanical faults as it is shown in figure 3-1[18]. These faults can be detected by several techniques such as MCSA, vibration monitoring or AI methods. In this section, a review of the most common faults and its related vibration frequencies will be studied.

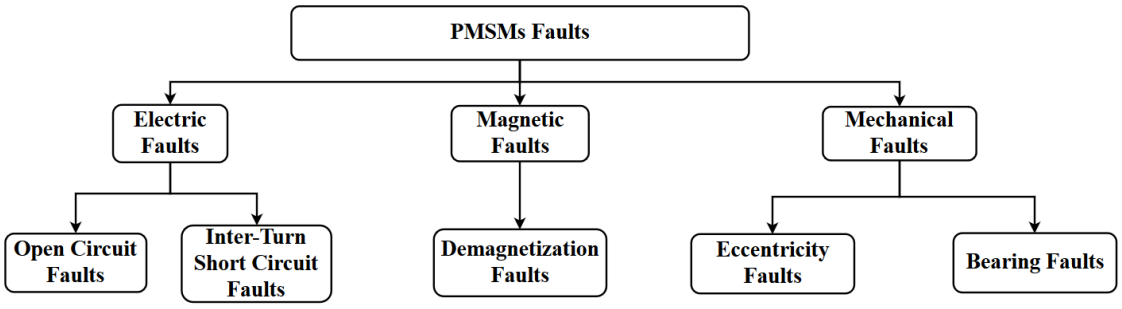

Figure 3-1: PMSMs Faults Classification

3.4.1 Electric Faults

The two major types of electric faults in PMSMs are open circuit faults and inter-turn short circuits faults. The open circuit fault is caused by a broken winding which avoids the circulation of the current through that phase. This has a large effect in

the performance of the machine which can even prevent it from starting. The inter-turn short circuit in the stator windings of the machine is caused by overloading the machine and high temperatures. The insulation of the coils breaks causing the current path to lose turns and lower the inductance and performance of the machine and increases current harmonics, torque ripple and vibrations. The related frequencies for this kind of faults are shown in equation (3.8), where Z is the number of slots, p the pole pairs, f_s is the source frequency or electric speed of the machine in synchronous operation and k is an integer number.

$$f_{slot} = f_s\Big(k\frac{Z}{p} \pm 1\Big) \tag{3.8}$$

3.4.2 Magnetic Faults

The main magnetic fault in a PMSM is magnet demagnetization fault. The magnets of the motor can be demagnetized due to high temperatures or high stator currents or short circuit currents. These faults result in an asymmetric flux distribution in the airgap leading to high vibrations. This fault creates an unbalanced magnetic pull and the related vibration frequencies appear in the low frequency region [19] of equation (3.9).

$$f_{demag} = f_s\Big|1 \pm \frac{k}{p}\Big| \tag{3.9}$$

3.4.3 Mechanical Faults

Mechanical faults are subdivided into bearing faults and eccentricity faults. Bearings may fail due to fatigue and ageing, but vibrations, improper assembly and unbalanced loading contribute to premature fails. The eccentricity faults cause large vibrations in the machine. Related frequencies for eccentricity faults are shown in equation (3.10).

$$f_{eccentricity} = f_s\Big(1 \pm \frac{2k-1}{p}\Big) \tag{3.10}$$

3.5 Other diagnosis methods

Vibration monitoring is one of the most used diagnosis techniques in the industry, but there are other diagnosis techniques that are widely used in PMSMs. The most common ones are: MCSA, magnetic field monitoring, temperature monitoring and learning based techniques or neural networks.

3.5.1 MCSA

Motor current signature analysis uses the spectral harmonic content in phase currents of the motor in order to detect motor faults. It is demonstrated that this method can be used to detect electric faults [20] but, also, magnetic faults [21] and mechanical faults [22].

3.5.2 Back Electromotive Force

The induced back electromotive force of a PMSM is produced by the movement of the rotor field respect to the stator windings. In the case of partial demagnetization faults, the rotor field has an uneven pattern which causes the Back-EMF voltage reduction when the faulty magnet passes in front of the studied pole [23]. This causes the presence of fractional harmonics in the Back-emf frequency spectrum which can be used to detect this kind of faults.

3.5.3 Zero Sequence Voltage

It is well known that stator current harmonics are affected by the bandwidth of the current control and inverter. Furthermore, in some machine arrangements, partial demagnetization faults do not produce additional harmonics in the current. In that case, other diagnosis methods must be used in order to detect this kind of faults. The zero sequence voltage monitoring is proposed in [24] where the fault severity is manifest by a developed index.

3.5.4 High Frequency Signal Injection

The signal injection techniques are able to detect motor asymmetries which can be used to estimate machine parameters such as rotor position, or it can be used to detect faults which causes asymmetries in the machine such as demagnetization faults. In [25], the variation in the magnetic saturation due to demagnetization is used and studied through current measurements as a demagnetization fault indicator.

3.5.5 Magnetic Field Monitoring

The magnetic field of a PMSM is produced by the rotor magnets and stator currents, therefore any change in these parameters is susceptible to be detected with magnetic field monitoring. This method is used to detect rotor magnets demagnetization [26] and rotor static and dynamic eccentricities [27] [28].

3.5.6 Temperature Monitoring

Temperature in a PMSM is an important parameter to take into consideration in order to prevent stator insulation failures and rotor magnets demagnetization. The temperature can be measured or estimated with sensorless estimation techniques. The interest in temperature estimation techniques has increased recently in the field of PMSMs for electric vehicles in order to monitor the motor temperatures without adding expensive temperature sensors [29] [30].

3.5.7 Neural Networks

During the recent years, the machine learning techniques have been improved and introduced in machine control and condition monitoring with a reduced human intervention [31]. Specifically, neural network techniques use different machine variables to classify the behaviour of the motor into the healthy or the different faulty operations [32] [33].

This neural network must to be trained with some data related with healthy motor behaviour and, in order to classify the fault type, data of operation under the different

faults must be provided. After the neural network is trained, it should be capable of distinguish between those operation conditions.

3.6 Vibration diagnosis in other machines

The diagnosis of electric machines has received a lot of attention, not only in PMSMs but also in IMs, Brushless DC Machines and DC Machines.

3.6.1 Induction Machine

A lot of research has been made in IMs condition monitoring because they have been massively used in the industry since long time ago. Vibration and sound monitoring is widely used for condition monitoring in these machines, the vibration spectra can be used to detect faults such as: voltage imbalance, rotor bar problems, voltage distortion or inverter faults [34], airgap eccentricity [35] and bearing faults [36].

3.6.2 Brushless DC Machine

The Brushless DC Machines (BLDCs), like the PMSMs, have permanent magnets in its rotor which generate the rotor flux without any stator current. The difference between BLDCs and PMSMs is the stator winding pattern, making the Back-EMF of the BLDC trapezoidal while in PMSMs is sinusoidal. BLDCs exhibits higher torque ripples and vibrations than PMSMs, and vibration monitoring is not commonly used, but other diagnosis methods are proposed in the literature [37].

3.6.3 DC Machine

DC Machines are other kind of machines which are widely used in the industry due to its easier speed controllability. These machines need more maintenance than PMSMs due to the presence of its brushes which needed to commutate between one winding to another. These commutations can lead in vibrations and a premature fatigue failure.

The harmonic vibration spectrum of DC machines can be used to detect faults such as magnet defects and short circuit to collector [38].

3.7 Vibration control

The PMSMs have higher torque ripple and vibrations than IMs or DC Machines. The vibration is a major drawback for the use of PMSMs in applications where the load can not withstand those vibrations. Some of the applications where the minimization of vibrations becomes important are lifts, high precision robotic arms and escalators. However, there is not much research in vibration control or suppression in PMSMs. Nevertheless, there is some literature about general vibration suppression in torsional systems [39] and in two inertia systems [40] where some different control schemes are proposed and studied.

Torque ripple and vibration suppression in PMSMs is based in the subtraction of the undesired torque ripple to the torque command [3] with a feedforward control scheme or adding to the applied voltage to the motor a specific control action in charge of the vibration suppression.

In order to achieve vibration suppression in PMSMs, the only controller used in the literature is the repetitive controller, which takes the advantage of the periodic behaviour of the vibrations and torque ripples to compensate them. Using this repetitive controller the vibrations of the machine can be reduced component by component with the control scheme shown in figure 3-2 [41]. Furthermore, some improvements have been developed to the control scheme paralleling the auto-tuning algorithms [42].

In those papers the vibration is measured with an acceleration sensor, but the acceleration signal is processed through a Fast Fourier Transformation (FFT) and it is not directly feed into the repetitive controllers. The FFT provides the information of the acceleration signal in frequency components and amplitude, losing the phase information. In order to compensate this phase lag, a time leading gain K_2 is used.

In this work, a new implementation for this feed forward scheme is proposed. The

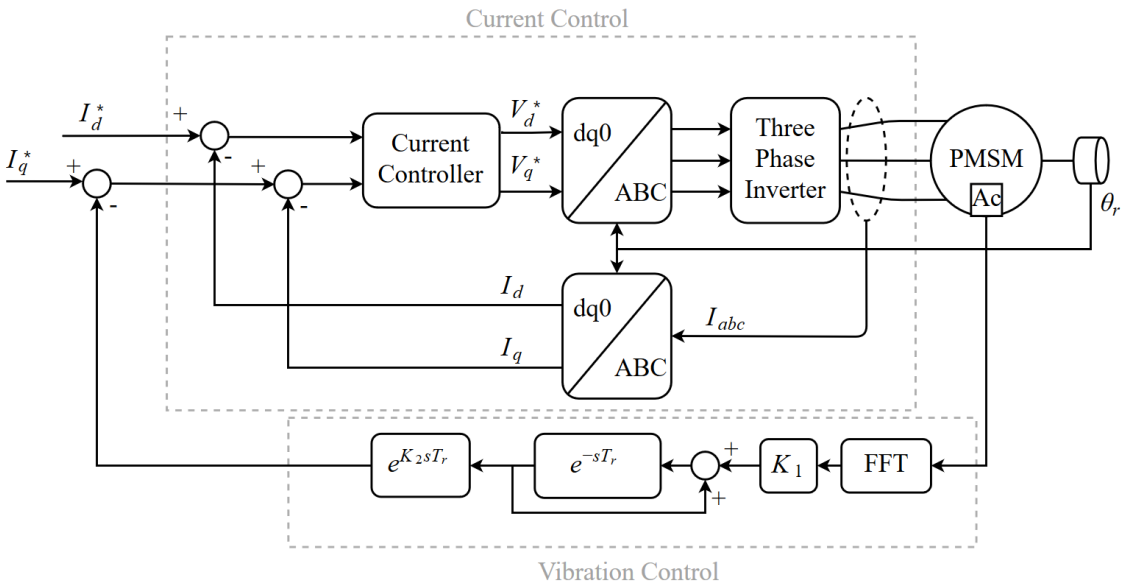

Figure 3-2: Feedforward repetitive controller scheme

vibration signal is rotated and filtered with a low pass filter at the desired cancellation frequencies. The filtered signal is used by two Perturb and Observe (P&O) algorithm which set the relative phase angle (respect the rotor angle) and the magnitude of the injected signal. The injected signal is fed into the i_q current command in order to compensate the vibrations or torque ripples. The proposed control scheme is shown in figure 3-3.

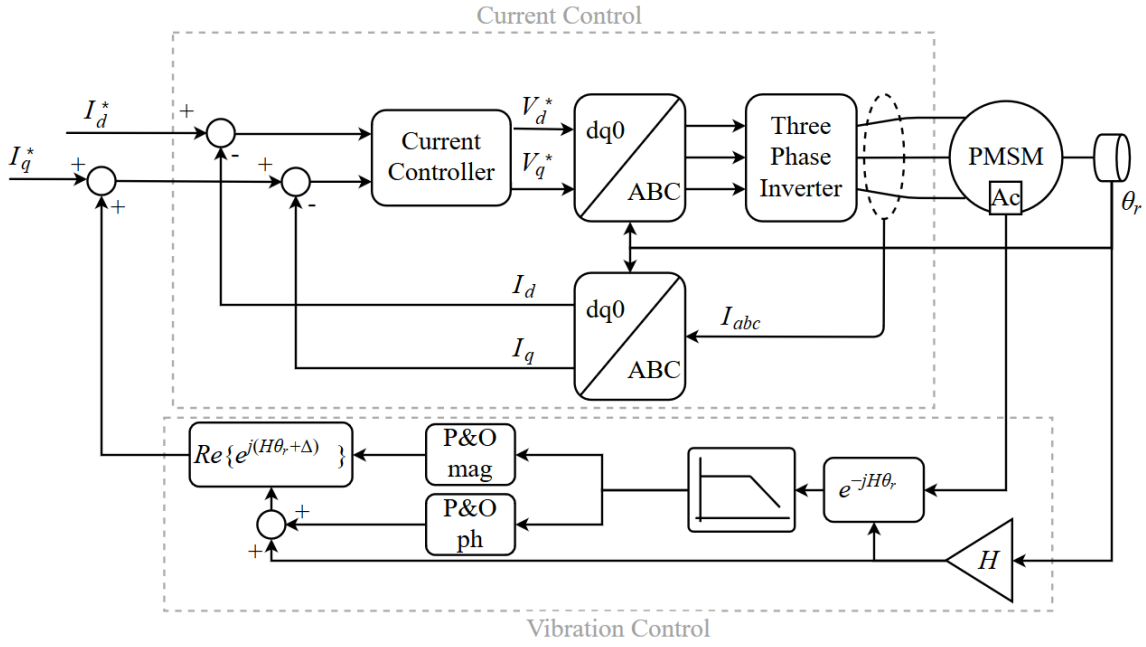

Figure 3-3: Proposed feedforward control scheme

Chapter 4

Vibration Measurement System

The vibration measurement system must be composed at least by an acceleration sensor, which will generate the acceleration signals, a control unit, which will acquire the signals generated by the acceleration sensor, and a power supply to provide voltage and current to the sensor and control unit.

In this work, in order to fulfil the objectives, two three-axis accelerometers are used (analog and digital) in order to make a comparison of the vibration spectrum measured by them. Furthermore, a microcontroller is used in order to acquire the sensor signals and to send the information to a computer or to the motor control circuit. The microcontoller will also handle four memories used to store the measured data while the communication with the computer or motor control is not available. In order to transfer the information from the microcontroller, a wireless transmission system is used. Finally, the power supply will consist of a voltage regulator, which will fed all the system with the same voltage level (3.3 V). This voltage regulator will allow the system to be powered by a battery or an external DC power source. This system arrangement can be seen in figure 4-1.

All these components make the vibration measurement system a versatile prototype which can be easily attached to a surface to retrieve the vibration information and transmit that information in real time to a PC for its on-line or off-line analysis.

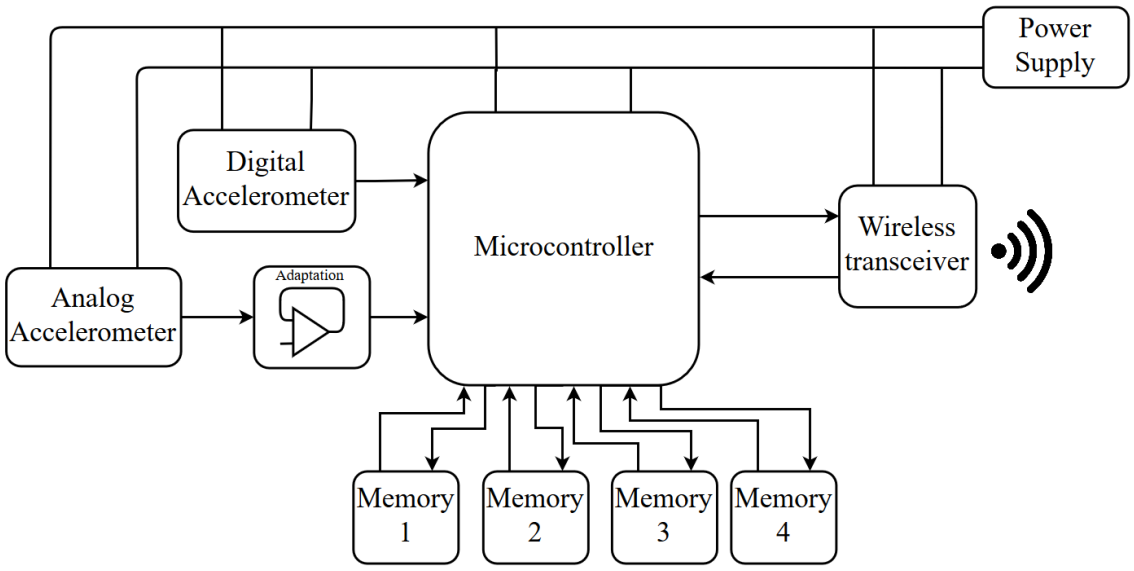

Figure 4-1: Vibration Measurement System scheme.

4.1 Sensors

The sensors necessary to retrieve the vibration data are acceleration sensors. In this case, a Microelectromechanical System (MEMS) accelerometer is selected due to its better characteristics at low frequencies measurements compared with other technologies such as piezoelectric accelerometers.

As it has been said, two accelerometers are needed for this prototype, one analog accelerometer and one digital accelerometer. In order to minimize the differences between the sensors and make a fair comparison, both of them are selected from the same brand: Kionix. Other characteristics to take into account to select the acceleration sensors are:

- Span and Resolution: The span of a sensor is the range between the lowest and the highest value that it can measure. In the case of accelerometers, usually the different ranges that can be found are given by $\pm 2^n$ (± 1, ± 2, ± 4, ...), being n a natural number. The resolution is the number of different values that the measure can get. In theory, for an analog sensor the resolution is infinite and any variation is proportionally applied to the sensor output signal. For a digital

sensor, as the resolution is finite, the span and resolution values will define the minimum change that can be measured. This minimum change is called Least Significant Bit (LSB) and it is calculated in equation (4.1).

$$LSB = \frac{Span}{Resolution} \tag{4.1}$$

For our system this is a critical characteristic because accelerations produced by torque ripples are small and a very small LSB will be needed in order to correctly measure it. In order to achieve this small LSB, the span will be low enough and the resolution will be as high as possible.

- Output Data Rate (ODR): digital sensors measure the data at discrete intervals. Usually, those intervals have a constant period and, therefore, a sampling frequency can be defined. The ODR is the number of samples that the sensor can get in one second, the sampling frequency. In analog sensors, the sampling frequency will be set by the analog to digital converter (ADC) (commonly built into microcontrollers) and it is limited by the analog output filter of the sensor or adaptation circuitry. For our system, the ODR will be as high as possible because the maximum vibration frequency that will be detected is limited to half of the sampling frequency according to the Nyquist-Shannon sampling theorem[43].

- Noise: noise is an intrinsic characteristic of any measurement system. There are several causes of noise: electromagnetic noise, switching devices, resistance thermal noise emission... The noise should be as low as possible in order to get accurate measurements. Furthermore, the total noise will be higher as higher is the bandwidth, thus a trade-off must be made between noise and sampling frequency.

The selected accelerometers and its characteristics are shown in table 4.1[44][45].

Table 4.1: Accelerometer characteristics.

	KX124-1051	KXTC9-2050
Technology	Digital	Analog
Range	$\pm 2g$, $\pm 4g$, $\pm 8g$	$\pm 2g$
Resolution/Sensitivity	16 bits	660 mV/g
ODR	50Hz - 25600Hz	-
Noise	$130\mu g/\sqrt{Hz}$	$125\mu g/\sqrt{Hz}$
Interface	SPI	Analog signal

4.2 Adaptation

Analog sensors usually need an adaptation circuit in order to be sampled by a microcontroller. This adaptation circuit can include a current to voltage converters, amplification circuits, integrators and other mathematical operations, anti-aliasing filters and others. In the case of the analog accelerometer, there is no need to add any amplification to the output voltage of the sensor. The adaptation circuit used in this prototype is an emitter-follower or voltage-follower which guarantees a high output impedance for the accelerometer sensor and minimizes the current flow while providing low input impedance and enough current to the analog to digital converter of the microcontroller.

The selected operational amplifier to implement the three voltage-followers (one per axis signal of the accelerometer) is the MCP6281.

4.3 Power Supply

The power supply must deliver voltage and current to the other subsystems of the prototype. The prototype is designed to have a single voltage level for the power supply of its elements for simplicity. The voltage level selected is the standard 3.3V which allows to supply MEMS accelerometers, microcontroller, memories and wireless transceiver. Therefore, a single output power supply is designed using a commercial buck converter.

The use of a buck converter allows the prototype to be fed from a wide range of input voltages. This can be used to feed the prototype for instance with a single

cell or two Li-Po battery or other DC power source. Furthermore, this increases the efficiency of the prototype compared with the use of a Linear Drop Output (LDO) voltage regulator, which is especially interesting with the use of batteries because it increases the autonomy of the prototype.

The selected commercial converter is the TPS62056, which has an input voltage range from 3.3V to 10V and a maximum output current of 800mA. Therefore, this device is more than enough to supply the prototype subsystems.

4.4 Memories

The memories are used to store the measure signals while the information can not be sent through the wireless communication. The memory size needs to be large enough to save at least one axis accelerometer's measurement cycle at the maximum sample. Furthermore, the interface between memories and microcontroler must be fast enough to transmit the information of a sampling period before the beginning of the next one.

The selected memory is the 23LC1024, which has a memory size of 1 Mbit and a SPI interface that will allow the fast data transfer with the microcontroller. In order to fulfil the data size requirement, four memories will be used in the prototype.

4.5 Wireless Transceiver

In order to send the acquired data to the PC or motor controller, a wireless transmission is used in this system. There are several wireless transmission technologies: radio frequency, bluetooth, WiFi... Among those technologies, the selected one for this project is WiFi due to its higher speeds and compatibility with PCs.

For this prototype, the commercial RN-171 will be used due to its simplicity of use. The RN-171 provides a WiFi interface with a built-in socket and TCP/IP protocol management, therefore the user only needs to send the data to the RN-171 through its UART interface.

The UART interface is an asynchronous communication system which uses two lines: one for receiving and one for transmitting. In order to use the maximum transmission speed of the RN-171 UART interface, two additional lines are used in order to implement the flow control capability of the UART interface. This capability allow the two connected devices to know when they are ready to receive new information, holding the transmission while the receiver is busy. Finally, the maximum transmission speed is selected: 230400 bits per second.

4.6 Microcontroller and Software

The microcontroller must handle the information flow: acquire the digital and analog acceleration signals, store them into the memories and send them to the WiFi module. Therefore, the minimum requirements for the microcontroller are: one ADC module with at least two independent sample-and-holds, one SPI module and one UART module.

The selected microcontroller is the dsPIC33EP128GS804 due to its CPU speed (up to 70 MIPS) and the fulfilment of the minimum requirements. This microcontroller has five 12-bit ADC cores, three SPI modules and two UART modules, therefore all requirements are fulfil and, additionally, one SPI module can be used for the digital accelerometer and other one for the memories, working at different frequencies.

The microcontroller program will manage the information flow, this program will be divided into two main tasks: acquisition and storage of the information and the transmission of that stored information to the PC. To store the information a software interface layer is developed which acts as a single First In First Out (FIFO) buffer. This buffer will be formed by some of the internal RAM memory of the microcontroller and the four external memories. A diagram of the information flow into the microcontroller is shown in figure 4-2.

The acquisition of the information is performed at a fixed sampling frequency and into an interrupt service routine raised by one of the timer modules. The operations that this task must deal with are: digital accelerometer read through SPI communi-

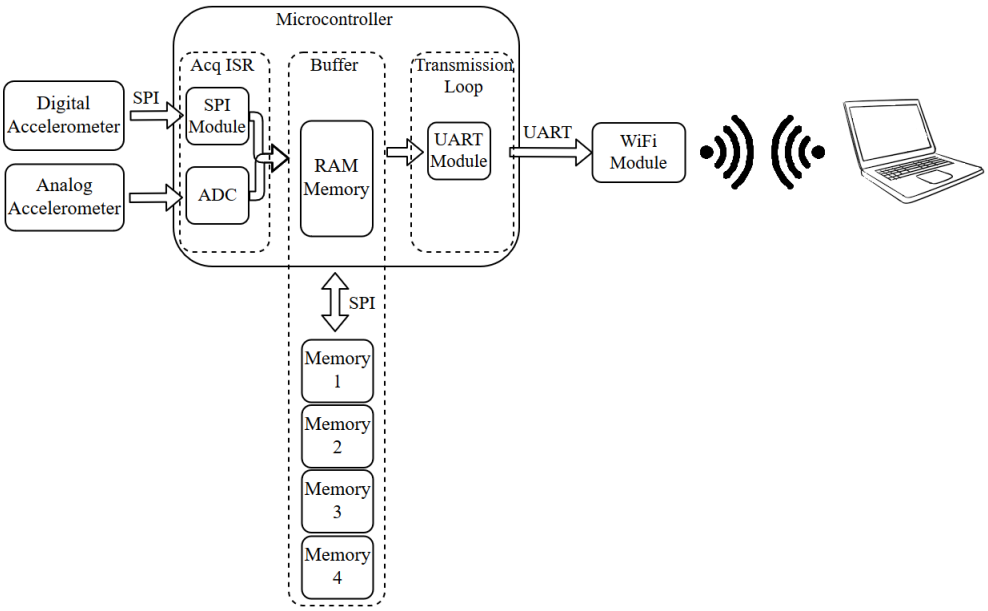

Figure 4-2: Information Flow Diagram.

cation, analog accelerometer read through ADC module, preparation of the signals to be stored and storing of the retrieved information in the buffer. An explanatory diagram of this task is shown in figure 4-3.

The transmission of the information to the wireless device will be implemented in the continuous execution loop, where if there is new information ready to be sent, the buffer will be read and it will be sent through the UART interface. An explanatory diagram of this task is shown in figure 4-4.

4.7 Manufacturing

Once all the elements of the prototype are selected to meet the requirements, a Printed Circuit Board (PCB) is designed and manufactured. Furthermore, a 3D socket is designed to hold the PCB and allow it to be easily attached to the motor or any other surface.

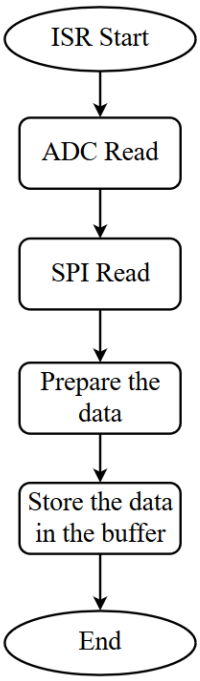

Figure 4-3: Acquisition program diagram.

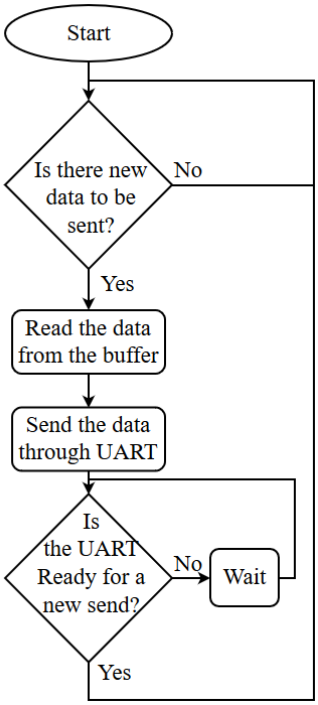

Figure 4-4: Continuous execution loop program diagram.

4.7.1 PCB

The PCB should be as small as possible because a reduced size will allow it to be more easily handle and placed in the motor frame. One additional constraint to build the PCB is the accelerometer axis alignment; axes of both accelerometers must be parallel in order to make a fair comparison of their signals, avoiding cross-coupling in their axes, in this way, measurements from one accelerometer in one axis can be directly compared to the ones in the other accelerometer.

In order to attach the PCB to the 3D printed socket some holes are drilled in the PCB and it will be fixed with screws. The designed PCB is shown in figure 4-5.

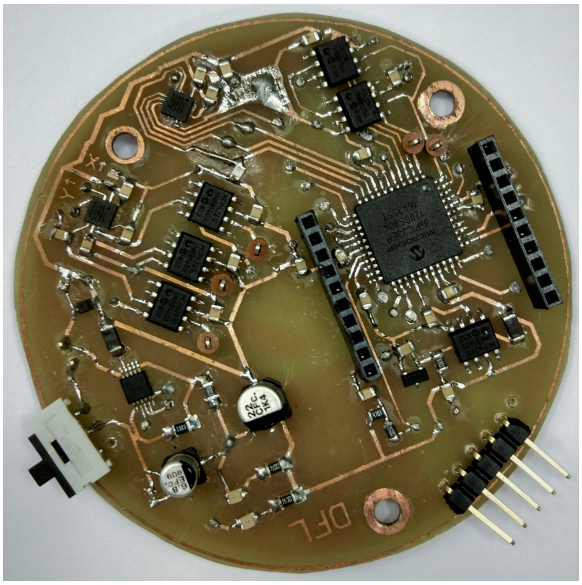

Figure 4-5: Final Printed Circuit Board.

4.7.2 3D printed socket

The 3D printed socket is designed to hold the PCB and to ease the attachment of the vibration measurement system to the motor frame or other surfaces. It has an interior cavity to place a small battery or to connect the PCB to an external DC power source. There is an additional cavity for the memories placed in the bottom side of the PCB. It also has some holes for the screws used to fix the PCB.

Additionally, there is a cavity with the shape of a magnet which will be used to make a strong attachment with ferromagnetic surfaces, for instance the motor frame. The bottom part of the socket is shaped in order to accommodate the external radius of the motor frame or, also, flat surfaces.

The final 3D printed socket is shown in figure 4-6.

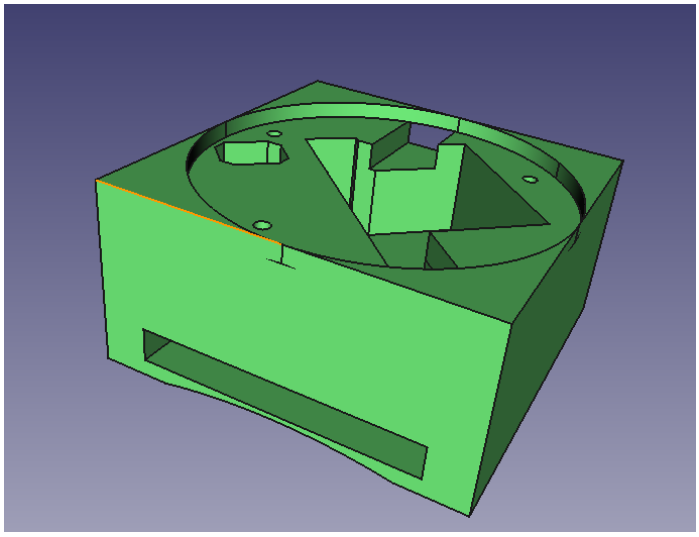

Figure 4-6: 3D printed socket model.

4.7.3 Final Prototype

Once the PCB and the 3D printed sockets are designed and manufactured, the final prototype is assembled and it is shown in figure 4-7.

4.8 PC data acquisition

In the PC side, a program was developed in order to retrieve the data sent by the prototype. The program handles a TCP/IP socket and reads the data stored in the socket receiving buffer. This data is stored in a text file for its later analysis in Matlab and, in addition, it is printed in a graphic in order to give instantaneous visual feedback to the user. The program interface can be seen in figure 4-8.

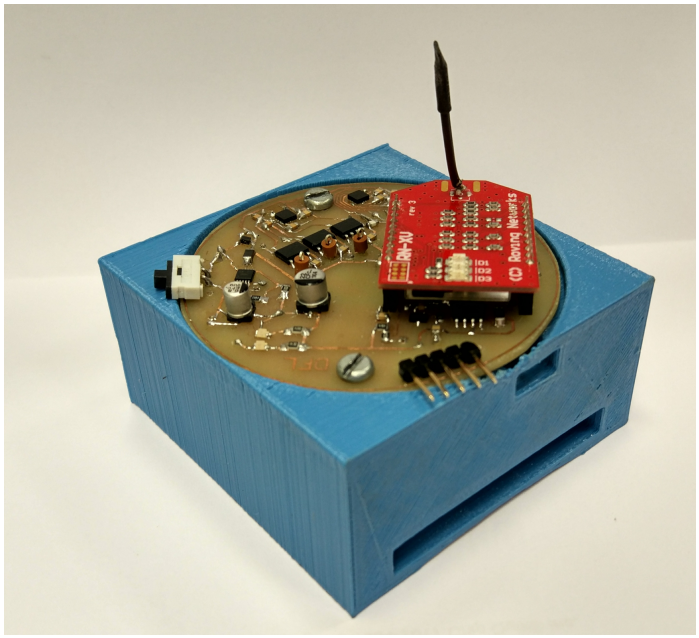

Figure 4-7: Photo of the final prototype.

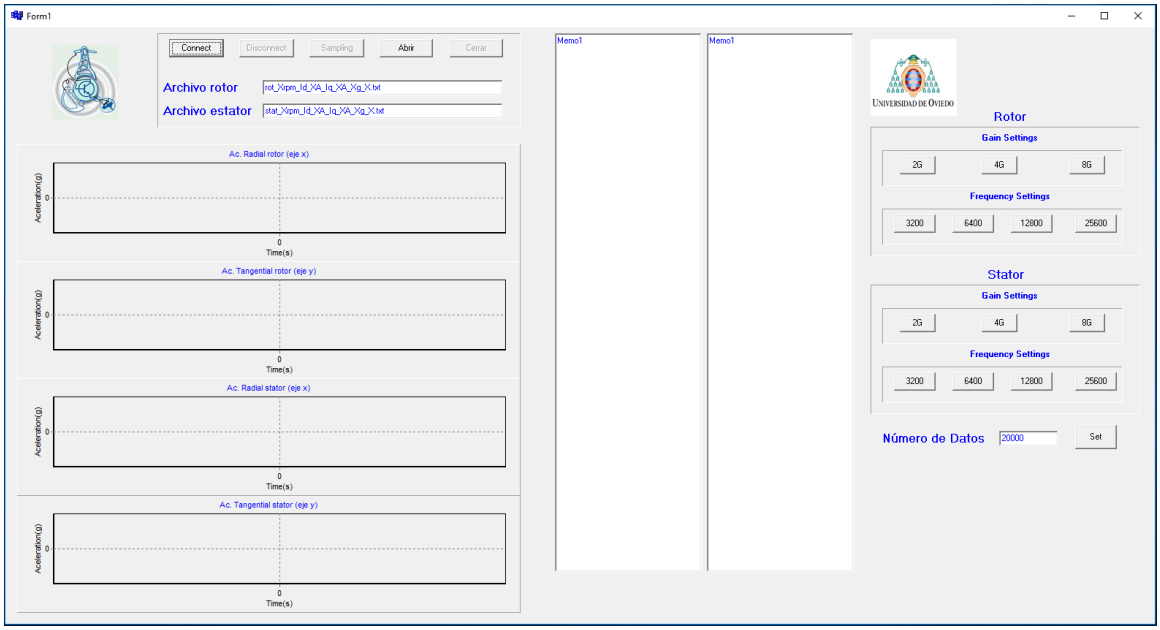

Figure 4-8: PC program interface.

Chapter 5

Experimental Results

In order to test the performance of the vibration monitoring system, the prototype is attached to the Interior PMSM (IPMSM) frame. The experimental setup consists of two PMSMs coupled through the shaft. The IPMSM where the prototype is placed is the "load machine", which has a current control loop to control the load torque, and the other PMSM is the machine which controls the rotational speed. The experiments are carried out at 200 rpm, since higher speeds would result in higher frequencies for the torque ripple, been filtered by the motor frame inertia. The characteristics of the IPMSM that is used in these tests are shown in table 5.1. In figure 5-1, a picture of this system is shown.

Table 5.1: IPMSM parameters.

Rated Power	7.5 kW
Rated Voltage	350 V
Pole pairs	3
Stator slots	36
Stator resistance	0.60 Ω
Magnetizing Inductance	0.03315 H
Stator leakage inductance	0.0022 H
Permanent magnet flux linkage	0.176 Vs

The power system supplying these machines consist of one rectifier, one DC/DC converter and one inverter for each machine. The connection scheme of this power system is shown in figure 5-2.

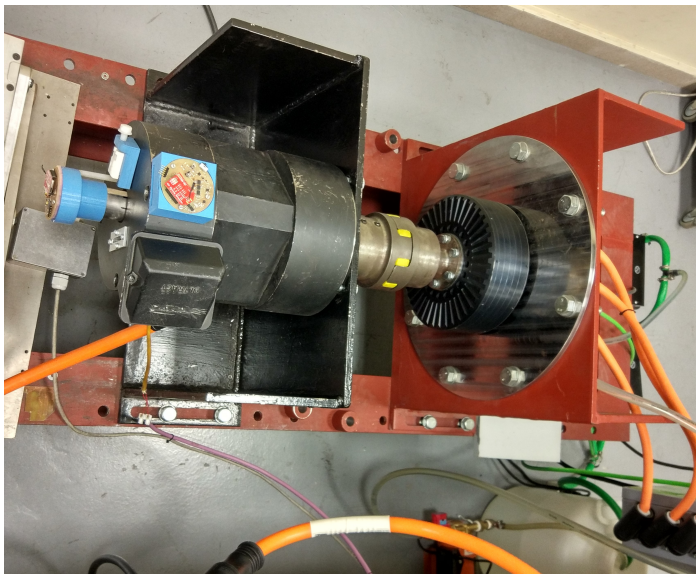

Figure 5-1: Picture of the experimental setup.

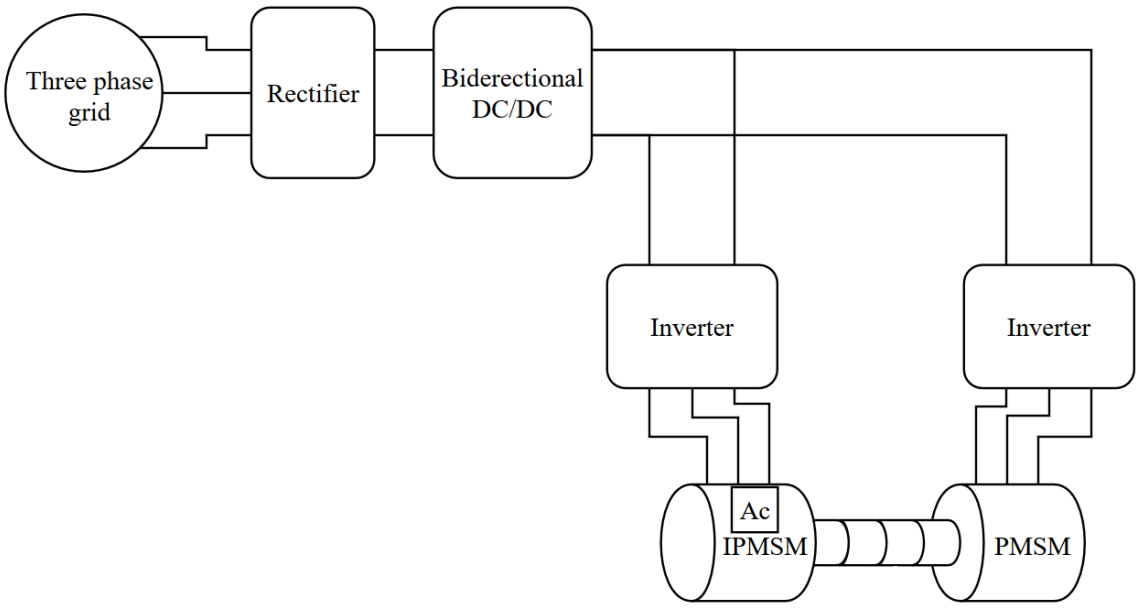

Figure 5-2: Power system scheme of the experimental setup.

5.1 Analog and Digital Comparison

Accelerometer manufacturers offer more digital than analog accelerometers because there is no need of design an adaptation stage, making it more attractive for customers. However, analog accelerometers can be used at higher sampling rates in some microcontrollers due to their high speed built-in ADC. On the other hand, these ADCs are usually limited to 14-bits resolution.

In order to test which is the most suitable accelerometer for the vibration measurement system a comparison is made in figure 5-3.

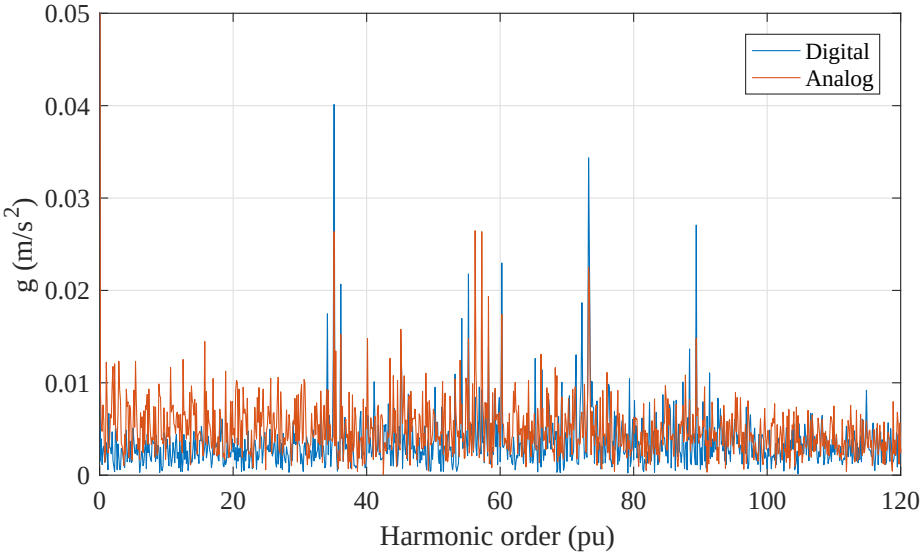

Figure 5-3: Analog and Digital accelerometers vibration spectrum.

Overall, both measurements are close to each other. The cogging torque harmonics 36th and 72th are correctly measured by both accelerometers, being the digital the most sensitive. In the low frequency region, from zero and up to the 36th order harmonic, the analog accelerometer exhibits higher ripple and higher mean value. This is due to the higher noise introduced by the adaptation state and the lower resolution of the ADC. For these reasons, the most suitable accelerometer for the vibration monitoring system is the digital accelerometer and it will be used for the following experiments.

5.2 Stator and rotor systems Comparison

A similar vibration measurement system was developed previously but it was designed for its attachment to the rotor of the machine [46]. It is of great interest to compare these two systems and state the benefits and drawbacks of both of them. A comparison of the vibration spectrum is shown in figure 5-4.

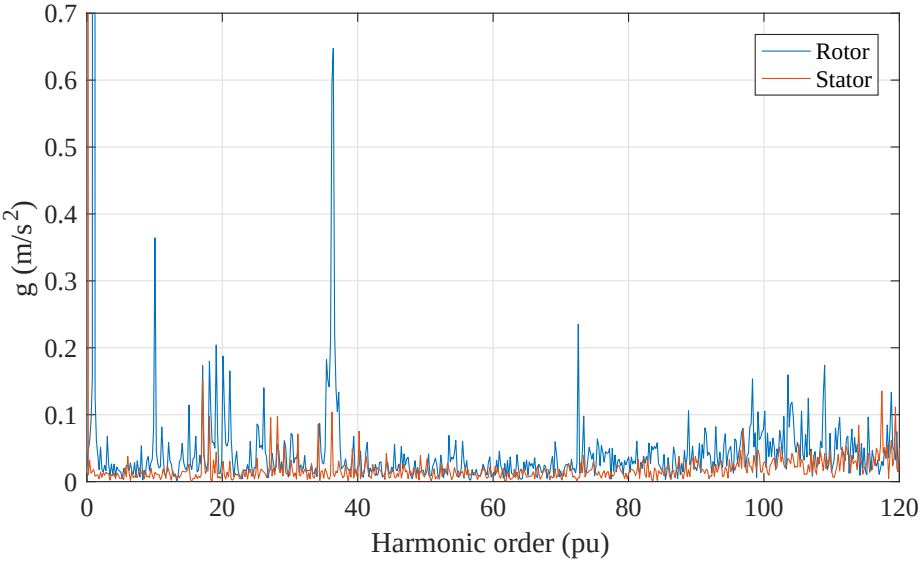

Figure 5-4: Rotor and stator vibration measurement systems comparison.

The first difference in the spectrum is the first order harmonic that appears in the rotor vibration measurement system spectrum due to the effect of the gravity in the accelerometer when the shaft rotates. This harmonic is ignored for FDD and vibration suppression; the same happens with the zero frequency magnitude of the stator system, which also corresponds to the gravity affecting to the accelerometer. Other interesting differences are the 36th and 72th cogging torque harmonics, which can be easily detected in the rotor system and they are above six times higher in magnitude. A 10th harmonic can be easily seen in the case of the rotor system, but it is not present in the case of the stator system, this harmonic corresponds to the number of poles of the other PMSM (speed control loop machine); it is transmitted to the rotor system through the shaft coupling but it is not transmitted to the stator system. Furthermore, below the 10th harmonic, some even harmonics are detected

by the rotor system; these harmonics corresponds to small eccentricity due to shaft coupling miss-alignment. This higher sensitivity can help detecting eccentricity faults.

Additionally, the rotor system has a complex attachment to the machine: it must be concentric with the shaft axis and fixed to its rotation. This implies that in order to add that system to a motor, an interruption in the production line must be programmed. On the other hand, the stator system can be attached to the machine without any change in the machine operation or interruption.

5.3 Mechanical Resonance

One of the major concerns when measuring vibrations in the machine is the mechanical resonance of the motor and bed. The resonance modes of the machine amplify the vibrations of those frequencies making them unsuitable for FDD because any small contribution at those frequencies lead to high measurements.

In order to estimate the mechanical resonance frequencies of the machine, a model is developed and simulated in a Finite Element Analysis (FEA) program. The IPMSM model in the FEA simulation is shown in figure 5-5. The estimated modal frequencies by the FEA simulation are shown in table 5.2

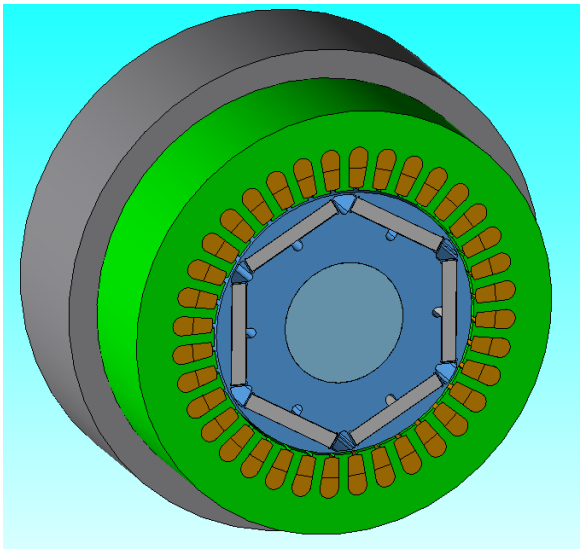

Figure 5-5: IPMSM model in the Finite Element Analysis program.

Table 5.2: Resonance Modes of the IPMSM.

Mode	Frequency
1	433 Hz
2	505 Hz
3	574 Hz
4	693 Hz
5	788 Hz
6	850 Hz
7	950 Hz
8	1092 Hz
several close modes	1150-2500 Hz

In order to verify FEA results, the stator vibration measurement system is placed in the machine, which is stopped. Then the motor bench is hit once with a metallic bar and the produced vibrations are stored and analysed. The time domain response and its spectrum are shown in figure 5-6.

The results show a first small component around 500 Hz, two medium size components around 650 and 750 Hz, and a large resonance from 1000 to 1500 Hz. The simulated and experimental results have some differences, but the modes around 500, 650 and 750 Hz are detected, and the large resonance from 1150 to 1500 Hz is also estimated but in the experimental results it decreases earlier at its higher frequencies and it does not reach 2500 Hz.

This resonance effect can be seen, also, in the normal operation of the vibration measurement system. In figure 5-7 the resonance effect in the normal operation is shown.

5.4 Motor Diagnosis

As it was stated before, this vibration measurement system should be able to work as FDD system analysing the vibration harmonic content. In order to test this capability, some test are performed.

First, the "Healthy machine" vibration spectrum is analysed and kept for comparison. After that, some faults are created in the machine, in this case, several

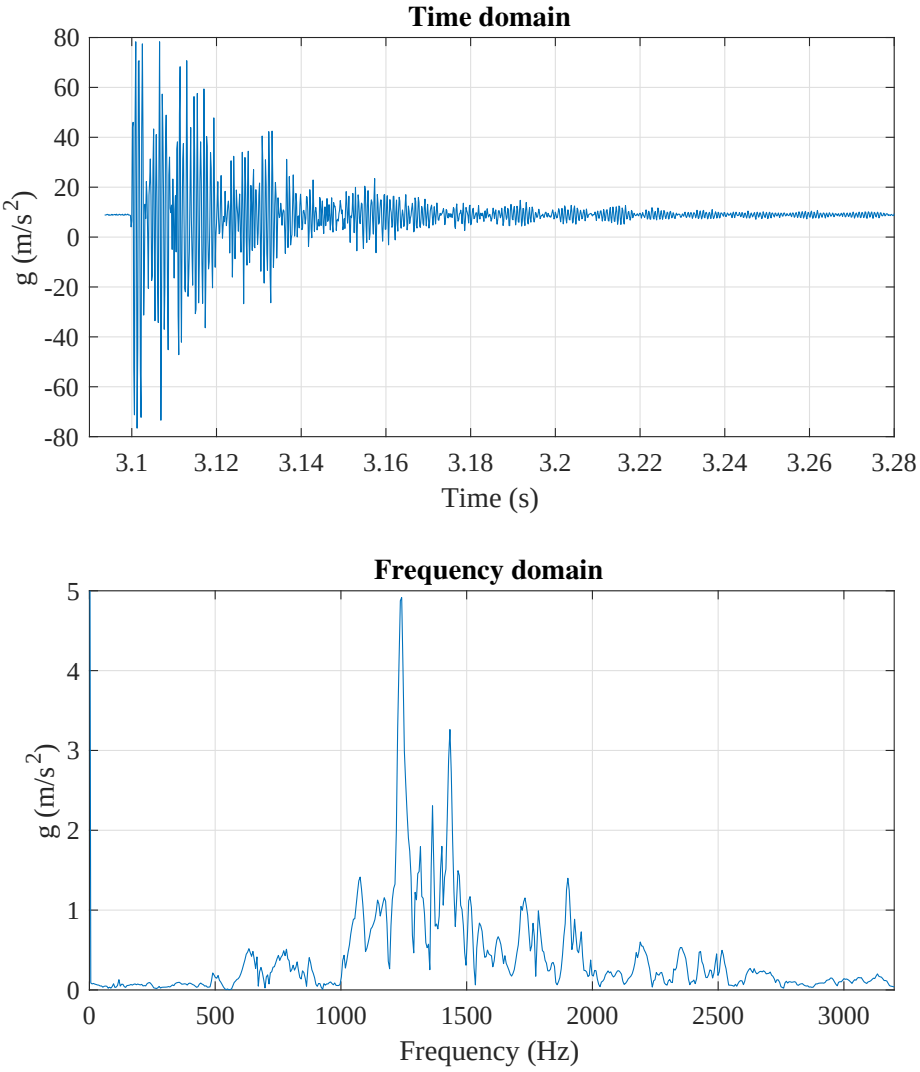

Figure 5-6: Vibration spectrum of mechanical resonance of the system.

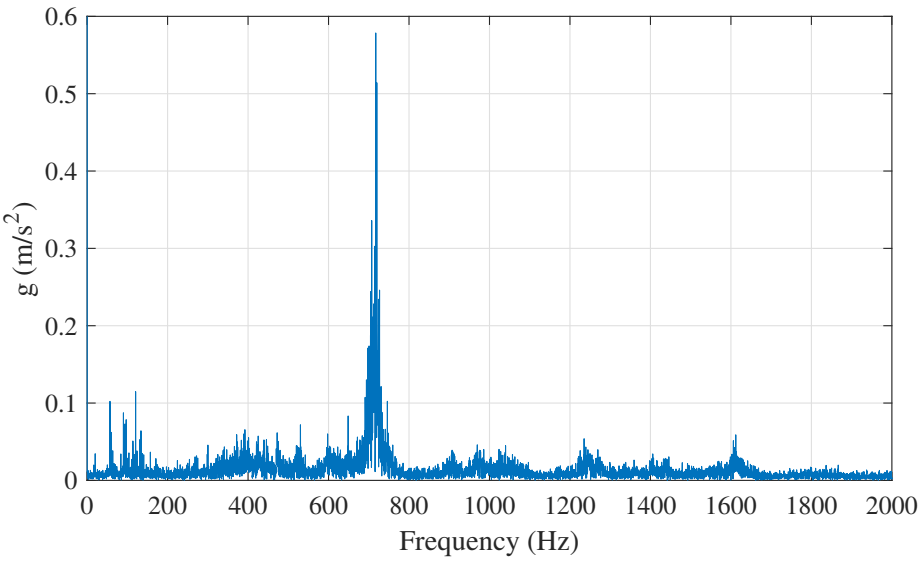

Figure 5-7: Vibration spectrum where the effects of the mechanical resonance appears.

demagnetization problems are studied. The healthy machine at no load vibration spectrum is shown in figure 5-8, and at nominal load ($i_q = 14A$) is shown in figure 5-9.

A demagnetization fault on a single magnet is simulated in the machine introducing a 50% magnetized magnet in the rotor. The vibration spectrum results without current injection are shown in figure 5-10. For this fault, as it was discussed before, some low frequency even harmonics are expected to appear. The results show no much difference in the low frequency region, only a small increase of the 4th harmonic, which is not very significant. Additionally, the 17th harmonic is greatly reduced and some side-band frequencies appear near the 36th harmonic (at 35th and 37th) while it is reduced.

In the case of nominal load current injection in the IPMSM, the vibration spectrum is shown in figure 5-11. The harmonic content of this test shows a large increase of the cogging torque side-band frequencies (35th and 37th) and also a large increase of the 72th harmonic, which is also related with cogging torque and stator slots effects.

The next test consists in simulating a demagnetization fault on three consecutive magnets. The fault is simulated introducing three consecutive magnets magnetized at 90% in the rotor of the machine. The results are shown in figure 5-12, where a

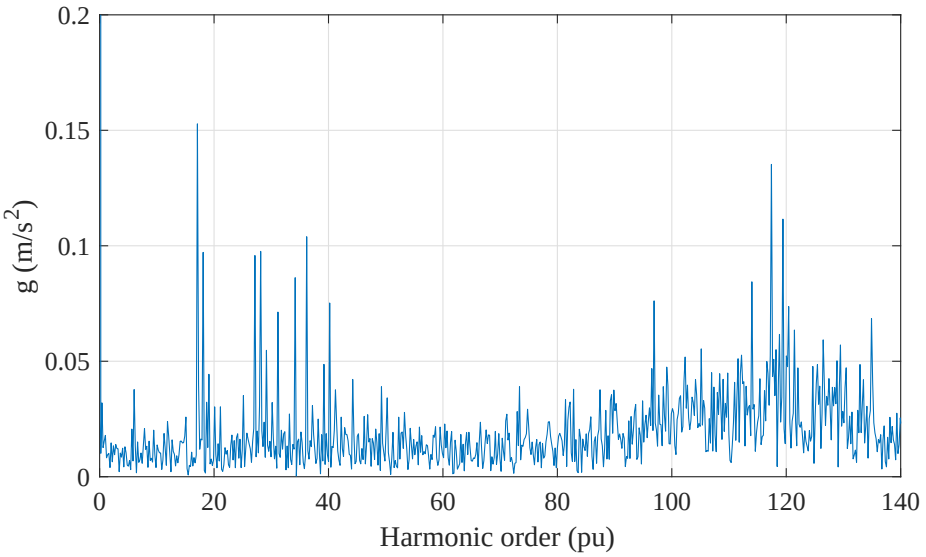

Figure 5-8: Healthy machine vibration spectrum with $i_{dq} = 0$.

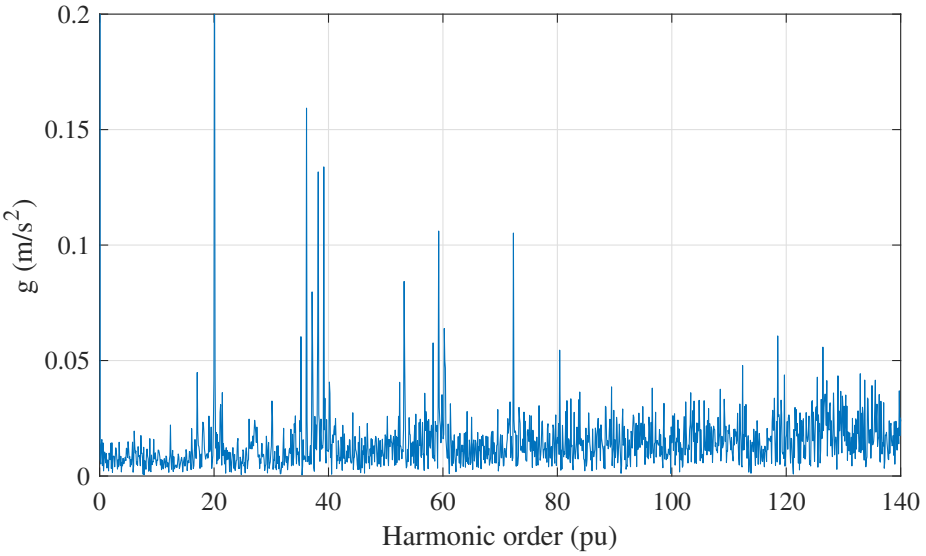

Figure 5-9: Healthy machine vibration spectrum with $i_q = 14A$ and $i_d = 0A$.

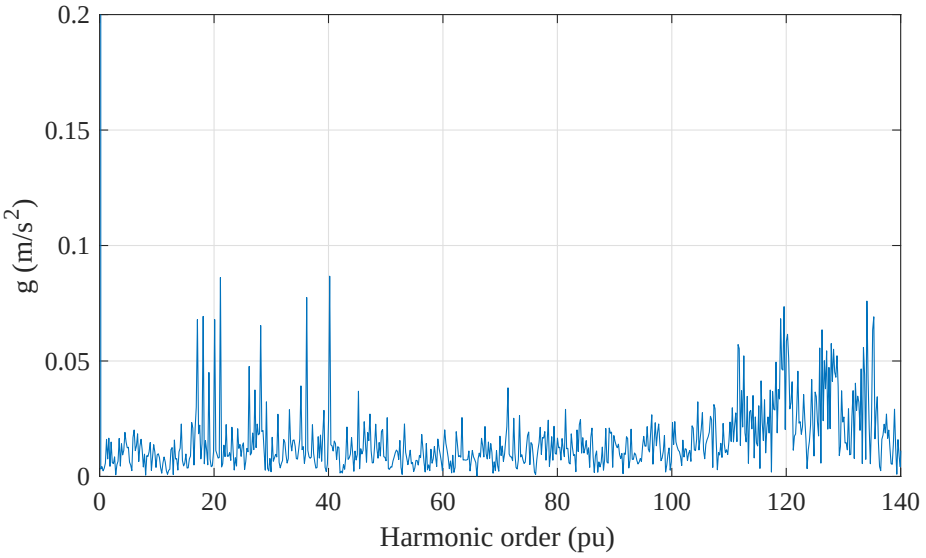

Figure 5-10: Partial demagnetized machine vibration spectrum for a single magnet with 50% magnetization with $i_{dq} = 0$.

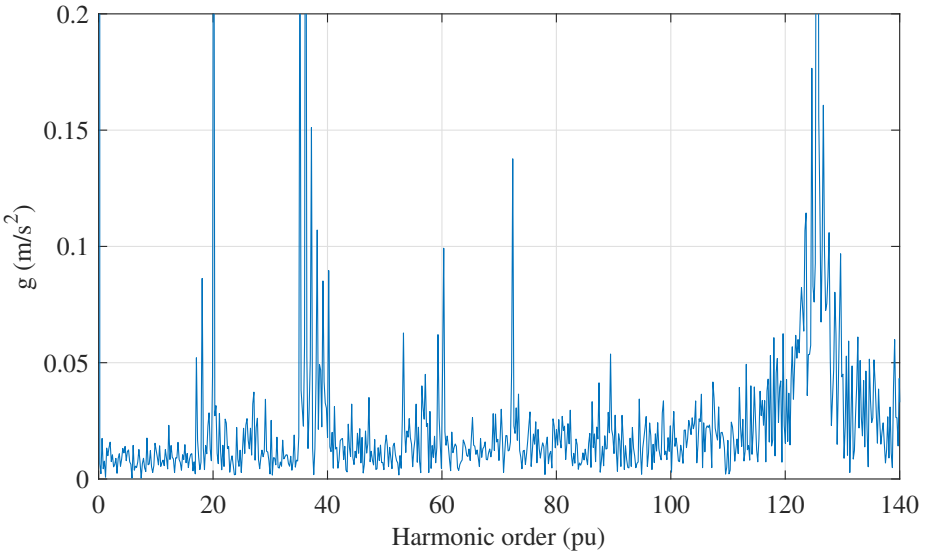

Figure 5-11: Partial demagnetized machine vibration spectrum for a single magnet with 50% magnetization with $i_q = 14A$ and $i_d = 0A$.

clear increase of the 72th harmonic appear and the 36th harmonic almost disappear. Additionally, a small increase in the even harmonics in the low frequency region appears.

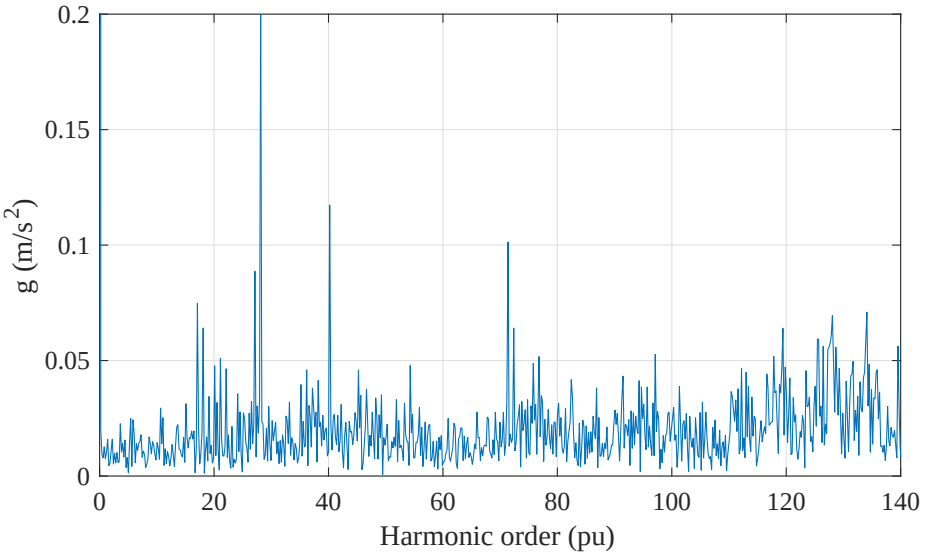

Figure 5-12: Partial demagnetized machine vibration spectrum for a three consecutive magnets with 90% magnetization with $i_{dq} = 0$.

For this fault, with nominal load current injection, the vibration harmonic spectrum is show in figure 5-13. In this case, the 36th harmonic appears again due to the effect of mutual torque ripple, the large side-band frequencies also appear with this fault.

The last fault is a demagnetization fault of all magnets set at 80% of magnetization. The vibration spectrum with no current injection is shown in figure 5-14. Results show lower cogging torque ripple (36th and 72th harmonics) and a decrease in other harmonics. Even so, the spectrum does not change in shape compared to the healthy machine case, difficulting the diagnosis.

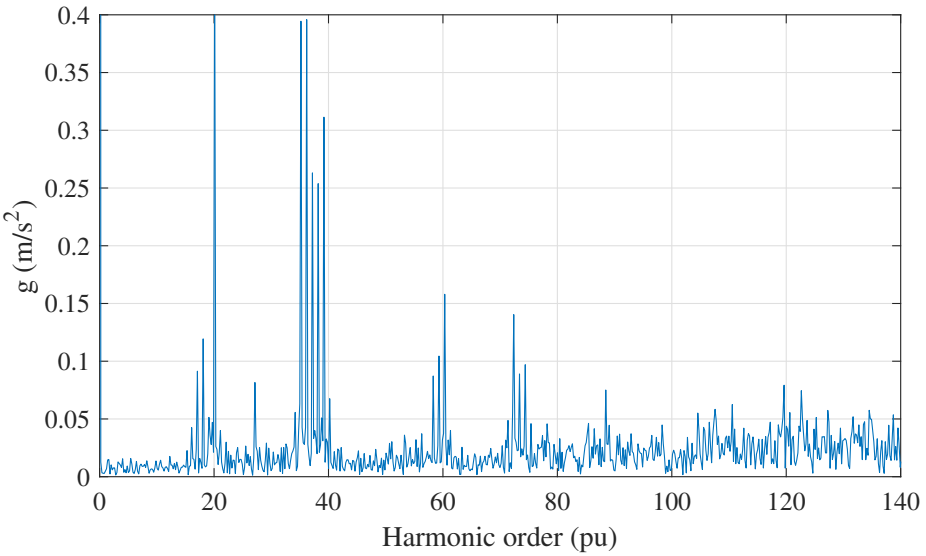

Figure 5-13: Partial demagnetized machine vibration spectrum for a three consecutive magnets with 90% magnetization with $i_q = 14A$ and $i_d = 0A$.

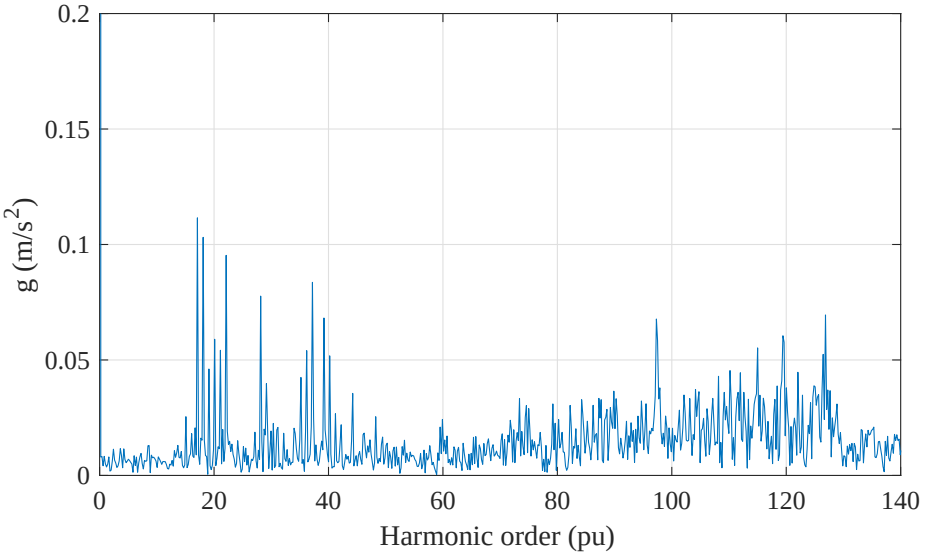

Figure 5-14: Machine vibration spectrum for all magnets magnetized 80% with $i_{dq} = 0$.

Chapter 6

Vibration Suppression Simulation

In order to test the proposed vibration suppression system, some simulations were carried out. In these simulations, the PMSM under test is a IPMSM model whose parameters are the same than the motor used in the experimental results and they are shown in table 5.1.

6.1 Machine Model

The model of the machine is based on the electrical model shown in equation (3.7) and in the torque model shown in equation (3.1). In order to account for cogging torque in the torque model and stator slotting in inductance variations in the electrical model, both being dependent on machine stator shape design, a cogging torque model and inductance variation model are developed.

Cogging torque model is pre-calculated and stored in a Look Up Table (LUT) and added to the simulation. The cogging torque force is a function of the rotor position, which is the input of the LUT. The function used to create the LUT values is shown in equation (6.1)[47], where i is a natural number, T_{sci} is the harmonic magnitude, p is the number of pole pairs, N_s is the slot number and θ is is the rotor angle.

$$T_{cog} = \sum_{i=1,2,3,\ldots}^{\infty} T_{csi} \frac{sin(2p\pi i)}{sin(\frac{2p\pi}{N_s})i} sin\Big(2pi\theta - \pi\frac{2p}{N_s}i\Big) \tag{6.1}$$

Calculated cogging torque waveform for this machine is shown in figure 6-1.

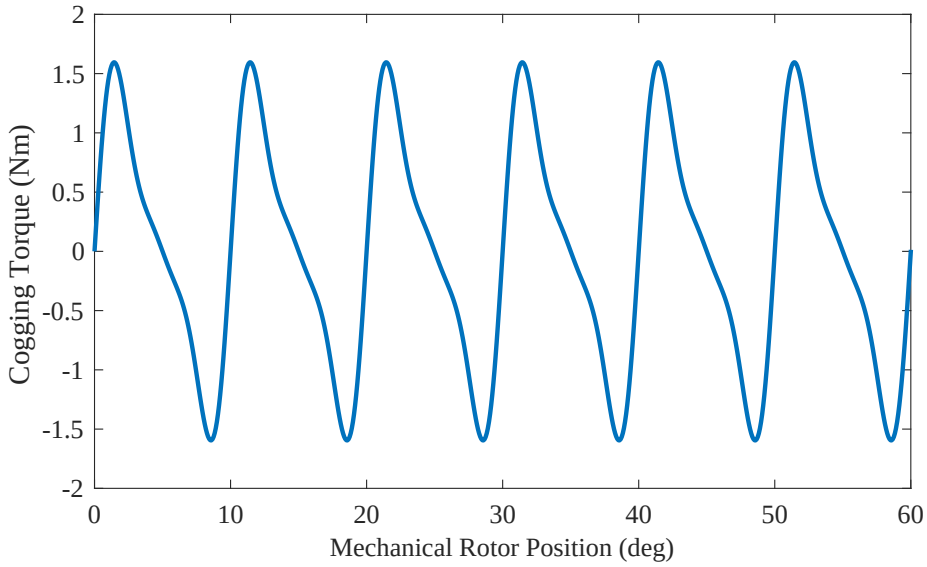

Figure 6-1: Cogging Torque waveform for the 6pole/36slot machine.

Inductance variation model due to stator slotting is based in the change of reluctance in the flux path when a stator slot passes in front of the rotor. This reluctance variation is expressed as an effective airgap length variation. Making the assumption that the flux describes a circular path to enter into the stator tooth when a stator slot is in its trajectory [48], the effective airgap length can be easily calculated. A explanatory scheme for this calculation is shown in figure 6-2.

This airgap variation is used to calculate the term $\frac{dL_{mdq}}{d\theta}$ in the electric model of the machine, the equation which relates that term and the airgap variation is shown in equation (6.2), where $\overline{L_{mdq}}$ is the mean value of the mutual inductance in the synchronous reference frame, $\overline{lg}$ is the mean airgap length and Δlg is the airgap length variation. From this equation, it can be seen that the derivative of the airgap length (slope) is also needed. The final airgap length variation and its derivative waveform, which will be saved in the LUTs, is shown in figure 6-3.

$$\frac{dL_{mdq}}{d\theta} = -\overline{L_{mdq}} \frac{\overline{lg} \frac{d\Delta lg(\theta)}{d\theta}}{(\Delta lg(\theta) + \overline{lg})^2} \tag{6.2}$$

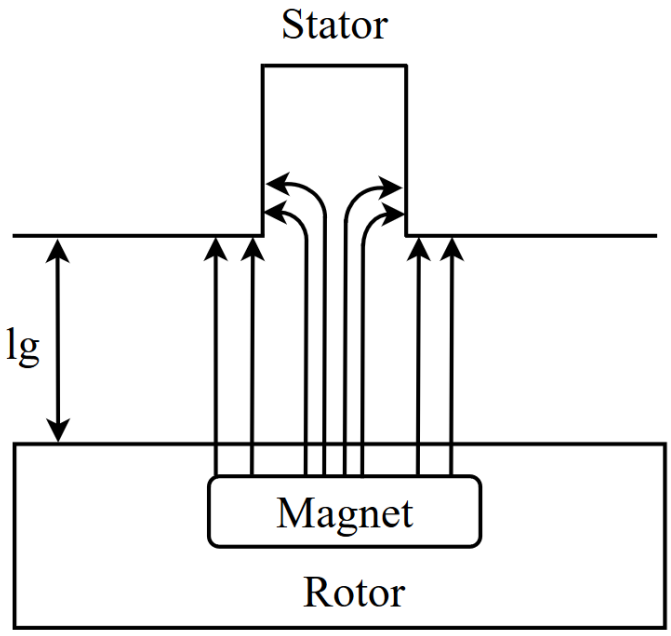

Figure 6-2: Flux path in a slot.

6.2 Simulation results

Simulations are performed in order to test the torque ripple harmonics that cogging torque and stator slots create, the results are shown in figure 6-4.

With these two sources of vibration, the proposed vibration suppression system (figure 3-3) is implemented and simulated. In figure 6-5, the achieved suppression of 36th and 72th harmonics in the output torque is shown, proving the validity of the method.

The P&O algorithm, implemented for angle and magnitude of the harmonics injected in the quadrature axis current, tracks the optimal values which minimize the output vibrations. The magnitude of the 36th harmonic of the torque ripple and the phase and magnitude of the current injected are shown in figure 6-6.

However, the current control loop bandwidth plays an important role in this vibration suppression scheme. The bandwidth used in these simulations is 500Hz, which is enough to cancel vibrations of this machine running at 10Hz, but at higher speeds the current control cannot track the frequency of the injected current signals correctly

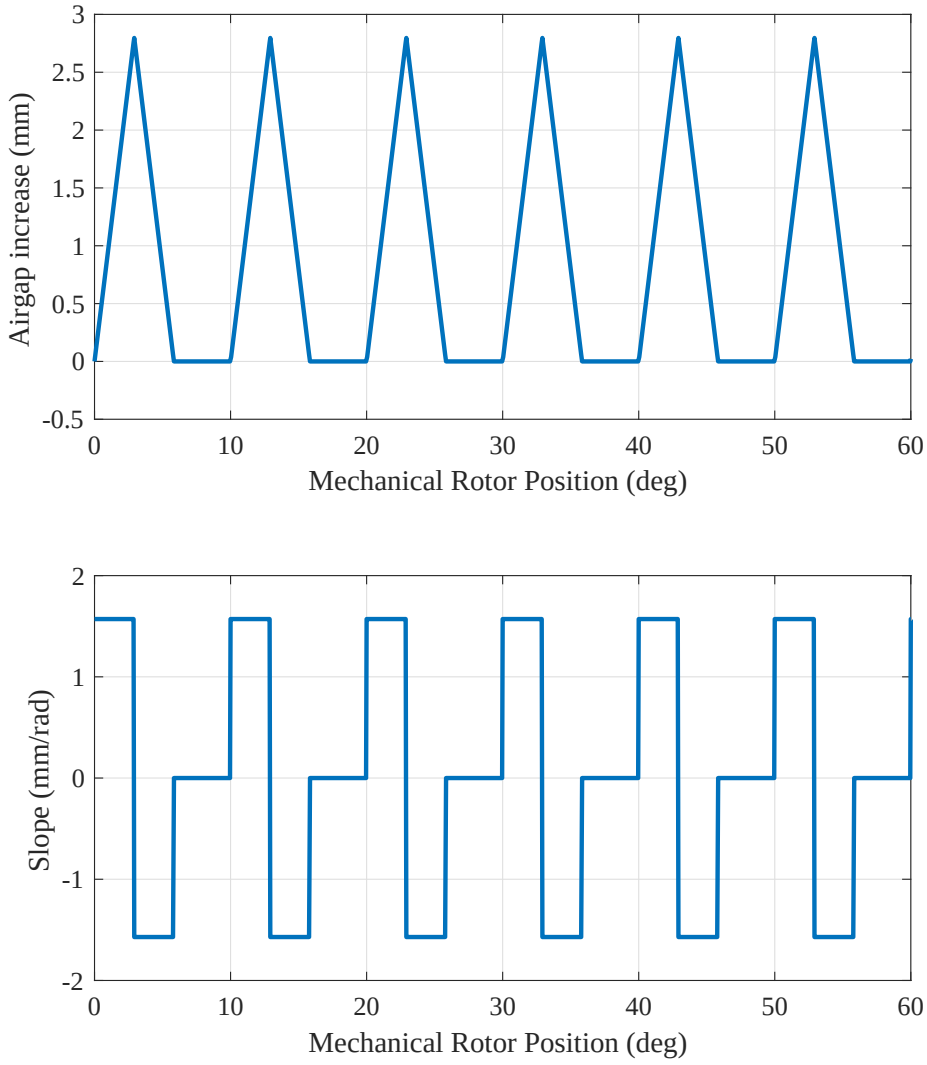

Figure 6-3: Airgap length variation and its slope.

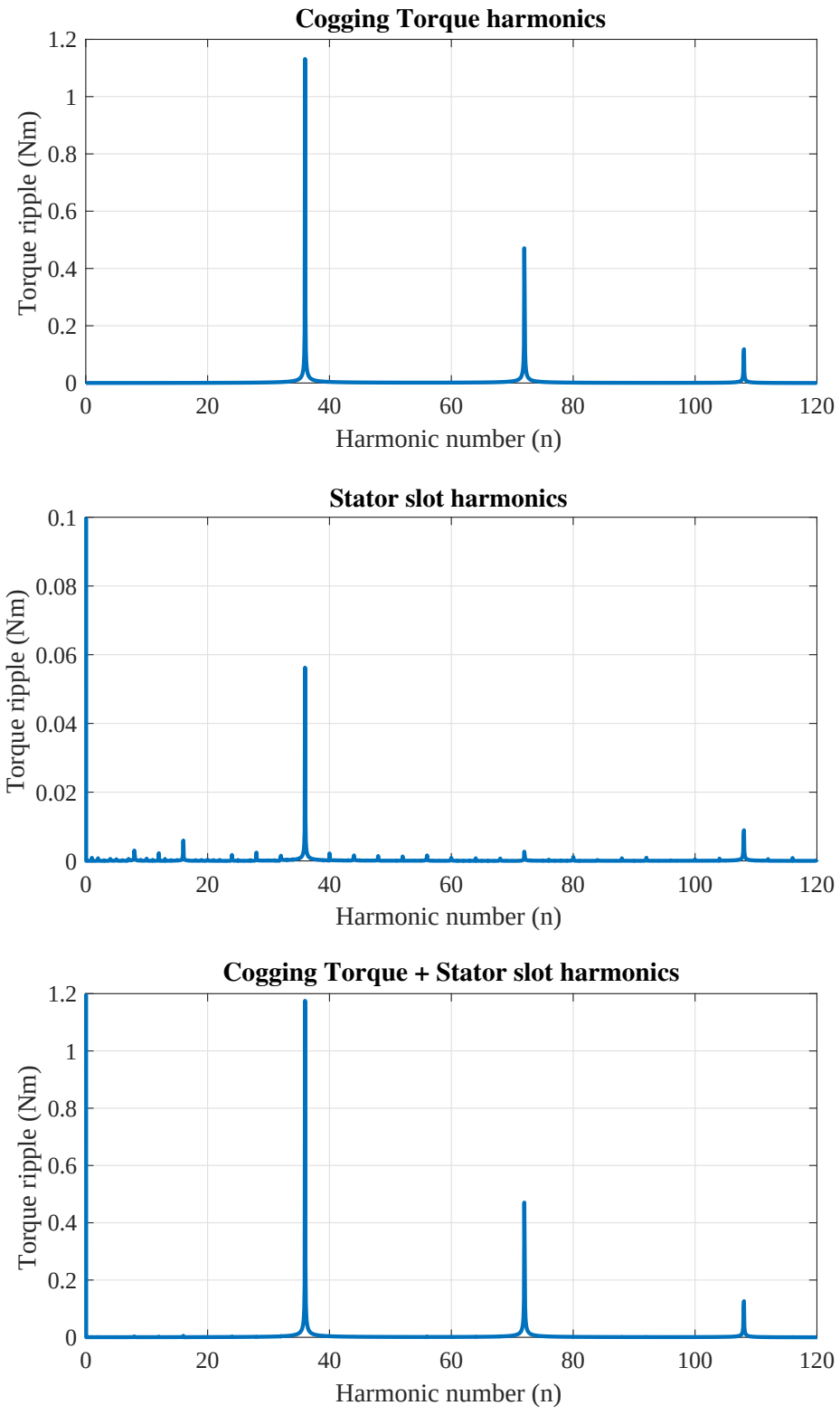

Figure 6-4: Torque ripple harmonics due to Cogging Torque, due to stator slotting and both effects.

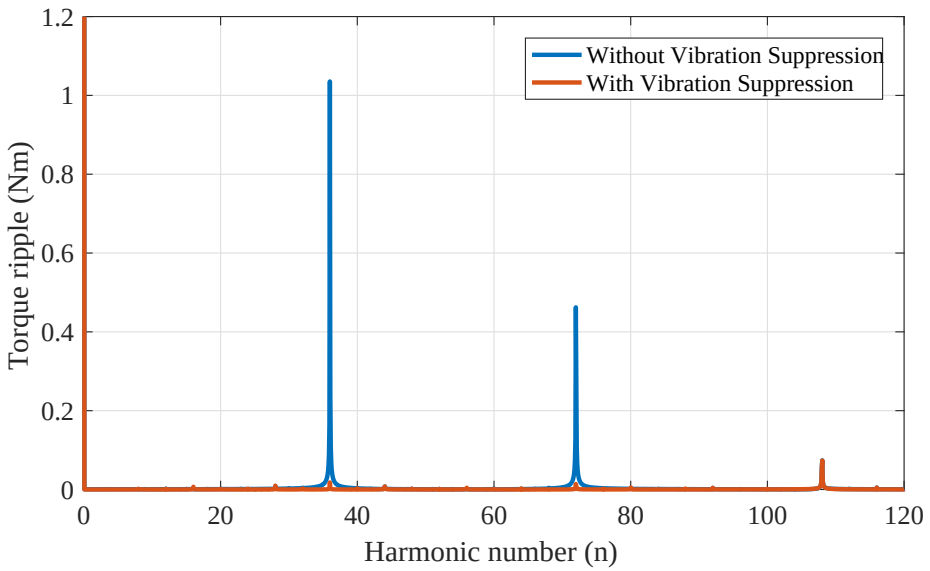

Figure 6-5: Torque harmonic suppression of 36th and 72th harmonics.

and, therefore, cancellation of those torque harmonics is not possible. Nevertheless, higher frequency torque ripples will be filtered by the machine inertia and will not lead into significant vibrations.

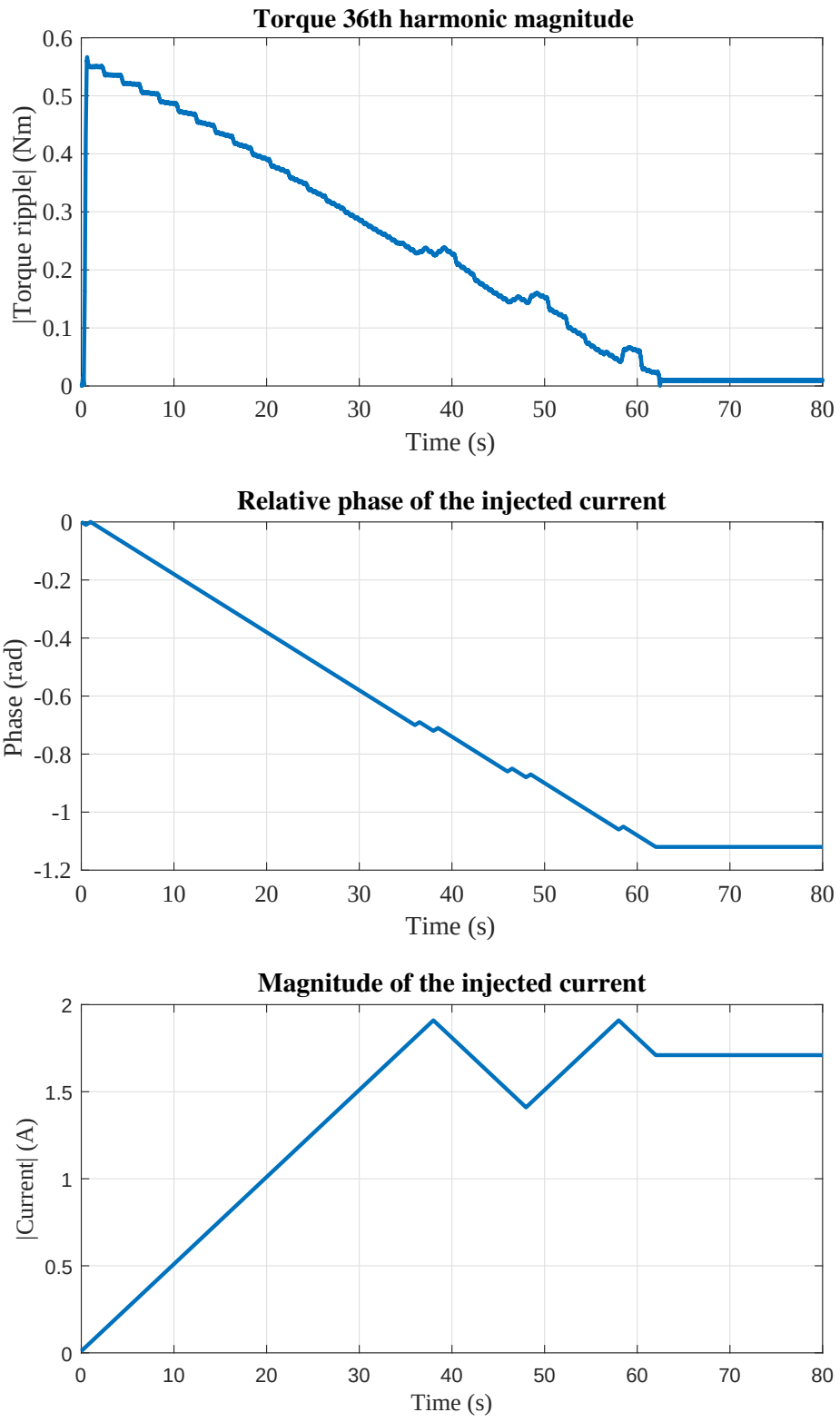

Figure 6-6: Perturb and observe phase and magnitude outputs by the 36th torque ripple harmonic amplitude.

Chapter 7

Conclusions

In this Master Thesis a new vibration measurement system is developed. The hardware and software of the system are optimised for the proper acquisition of vibrations in the stator of the machine. The system can be easily attached to the motor frame or any ferromagnetic surface without any interruption or change in the operating conditions of the machine thanks to its magnet and 3D printed socket.

This prototype has been tested in a real motor in order to validate its capabilities. The experimental results show that the vibration measurement system is able to detect partial magnetization faults analysing the harmonic content of the vibration spectrum. Furthermore, this prototype has been compared with the previous one developed for rotor measurements and its benefits and drawbacks have been stated.

Finally, a vibration suppression scheme has been proposed and validated through simulation. In this simulation, the cogging torque and the effect of stator slotting of the machine are modelled and included in the IPMSM model. The vibration suppression scheme showed the ability to reduce torque ripple harmonics and vibrations with P&O algorithms, which calculate the proper values for current injection to compensate those vibrations.

Chapter 8

Future Work

This work does not include a complete set of faults using the developed vibration measurement system, and the vibration suppression scheme has not been tested experimentally. The developed IPMSM model can be used to take into account eccentricity and magnet faults but the necessary software has not been implemented yet. Therefore, some of the future improvements of this master thesis are:

- Include eccentricity, single magnet magnetization and short-circuit effects to the simulated model in order to use it as validation tool for the experimental results.
- Make a complete set of faulty machine measurements where the three types of faults are tested: mechanical faults, magnetic faults and electric faults.
- Implement the proposed vibration suppression scheme in the real machine in order to validate it experimentally.

Bibliography

[1] Subhasis Nandi, Hamid A Toliyat, and Xiaodong Li. Condition monitoring and fault diagnosis of electrical motors—a review. *IEEE transactions on energy conversion*, 20(4):719–729, 2005.

[2] C Heising et al. Ieee recommended practice for the design of reliable industrial and commercial power systems. *IEEE Inc., New York*, 2007.

[3] Matthew Piccoli and Mark Yim. Cogging torque ripple minimization via position based characterization. In *Robotics: Science and Systems*, 2014.

[4] Shanming Wang, Jianfeng Hong, Yuguang Sun, and Haixiang Cao. Exciting force and vibration analysis of stator permanent magnet synchronous motors. *IEEE Transactions on Magnetics*, 2018.

[5] Masato Kanematsu, Takayuki Miyajima, Hiroshi Fujimoto, Yoichi Hori, Toshio Enomoto, Masahiko Kondou, Hiroshi Komiya, Kantaro Yoshimoto, and Takayuki Miyakawa. Suppression control of radial force vibration due to fundamental permanent-magnet flux in ipmsm. In *Energy Conversion Congress and Exposition (ECCE), 2013 IEEE*, pages 2821–2826. IEEE, 2013.

[6] Tao Sun, Ji-Min Kim, Geun-Ho Lee, Jung-Pyo Hong, and Myung-Ryul Choi. Effect of pole and slot combination on noise and vibration in permanent magnet synchronous motor. *IEEE Transactions on magnetics*, 47(5):1038–1041, 2011.

[7] Joachim Holtz and Lothar Springob. Identification and compensation of torque ripple in high-precision permanent magnet motor drives. *IEEE Transactions on Industrial Electronics*, 43(2):309–320, 1996.

[8] Alejandro J Pina Ortega. *Modeling and Analysis of Asymmetries in Permanent Magnet Synchronous Machines*. The Ohio State University, 2016.

[9] Z Azar, ZQ Zhu, and G Ombach. Influence of electric loading and magnetic saturation on cogging torque, back-emf and torque ripple of pm machines. *IEEE Transactions on Magnetics*, 48(10):2650–2658, 2012.

[10] Joachim Holtz. Initial rotor polarity detection and sensorless control of pm synchronous machines. In *Industry Applications Conference, 2006. 41st IAS Annual Meeting. Conference Record of the 2006 IEEE*, volume 4, pages 2040–2047. IEEE, 2006.

[11] Gabriel Gallegos-Lopez and Silva Hiti. Optimum current control in the field-weakened region for permanent magnet ac machines. In *Industry Applications Conference, 2007. 42nd IAS Annual Meeting. Conference Record of the 2007 IEEE*, pages 2154–2160. IEEE, 2007.

[12] Eric Favre, Larent Cardoletti, and Marcel Jufer. Permanent-magnet synchronous motors: A comprehensive approach to cogging torque suppression. *IEEE Transactions on Industry Applications*, 29(6):1141–1149, 1993.

[13] Thomas M Jahns and Wen L Soong. Pulsating torque minimization techniques for permanent magnet ac motor drives-a review. *IEEE transactions on industrial electronics*, 43(2):321–330, 1996.

[14] Vladan Petrovic, Romeo Ortega, Aleksandar M Stankovic, and Gilead Tadmor. Design and implementation of an adaptive controller for torque ripple minimization in pm synchronous motors. *IEEE Transactions on Power Electronics*, 15(5):871–880, 2000.

[15] Zhixin Li, Zhenfei Chen, Shufeng Lu, Shihai Yang, and Minrui Xu. Torque ripple reduction for non-sinusoidal back-emf permanent magnet synchronous machines with current harmonics. In *2016 19th International Conference on Electrical Machines and Systems (ICEMS), IEEE*. IEEE, 2016.

[16] ZQ Zhu and David Howe. Instantaneous magnetic field distribution in brushless permanent magnet dc motors. iii. effect of stator slotting. *IEEE transactions on magnetics*, 29(1):143–151, 1993.

[17] Thomas A Lipo. *Vector control and dynamics of AC drives*, volume 41. Oxford university press, 1996.

[18] Jingzhe Yang, Huiping Ye, Wei Zhou, et al. A review of permanent magnet synchronous motor fault diagnosis. In *Transportation Electrification Asia-Pacific (ITEC Asia-Pacific), 2014 IEEE Conference and Expo*, pages 1–5. IEEE, 2014.

[19] Zhi Yang, Xiaodong Shi, and Mahesh Krishnamurthy. Vibration monitoring of pm synchronous machine with partial demagnetization and inter-turn short circuit faults. In *Transportation Electrification Conference and Expo (ITEC), 2014 IEEE*, pages 1–6. IEEE, 2014.

[20] A Khlaief, M Boussak, and M Gossa. Open phase faults detection in pmsm drives based on current signature analysis. In *Electrical Machines (ICEM), 2010 XIX International Conference on*, pages 1–6. IEEE, 2010.

[21] Mohsen Zafarani, Taner Goktas, and Bilal Akin. A comprehensive analysis of magnet defect faults in permanent magnet synchronous motors. In *Applied Power Electronics Conference and Exposition (APEC), 2015 IEEE*, pages 2779–2783. IEEE, 2015.

[22] Bashir Mahdi Ebrahimi, Mehrsan Javan Roshtkhari, Jawad Faiz, and Seyed Vahid Khatami. Advanced eccentricity fault recognition in permanent magnet synchronous motors using stator current signature analysis. *IEEE Transactions on Industrial Electronics*, 61(4):2041–2052, 2014.

[23] J Urresty, Jordi-Roger Riba, and Luís Romeral. A back-emf based method to detect magnet failures in pmsms. *IEEE Trans. Magn*, 49(1):591–598, 2013.

[24] Julio-César Urresty, Jordi-Roger Riba, Miguel Delgado, and Luís Romeral. Detection of demagnetization faults in surface-mounted permanent magnet synchronous motors by means of the zero-sequence voltage component. *IEEE transactions on Energy conversion*, 27(1):42–51, 2012.

[25] Jongman Hong, Doosoo Hyun, Sang Bin Lee, Ji-Yoon Yoo, and Kwang-Woon Lee. Automated monitoring of magnet quality for permanent-magnet synchronous motors at standstill. *IEEE Transactions on Industry Applications*, 46(4):1397–1405, 2010.

[26] David Diaz, Daniel Fernandez, Yonghyun Park, Alberto B Diez, Sang Bin Lee, and Fernando Briz. Detection of demagnetization in permanent magnet synchronous machines using hall-effect sensors. *IEEE Transactions on Industry Applications*, 2018.

[27] Yonghyun Park, Daniel Fernandez, Sang Bin Lee, Doosoo Hyun, Myung Jeong, Suneel Kumar Kommuri, Changhee Cho, David Reigosa, and Fernando Briz. On-line detection of rotor eccentricity for pmsms based on hall-effect field sensor measurements. In *Energy Conversion Congress and Exposition (ECCE), 2017 IEEE*, pages 4678–4685. IEEE, 2017.

[28] BM Ebrahimi and J Faiz. Magnetic field and vibration monitoring in permanent magnet synchronous motors under eccentricity fault. *IET electric power applications*, 6(1):35–45, 2012.

[29] Razvan Mocanu and Alexandru Onea. Temperature estimation for condition monitoring of pmsm used in electric vehicles. In *Fundamentals of Electrical Engineering (ISFEE), 2014 International Symposium on*, pages 1–6. IEEE, 2014.

[30] Daniel Fernandez, Doosoo Hyun, Yonghyun Park, David Díaz Reigosa, Sang Bin Lee, Dong-Myung Lee, and Fernando Briz. Permanent magnet temperature estimation in pm synchronous motors using low-cost hall effect sensors. *IEEE Transactions on Industry Applications*, 53(5):4515–4525, 2017.

[31] I-Hsi Kao, Wei-Jen Wang, Yi-Horng Lai, and Jau-Woei Perng. Analysis of permanent magnet synchronous motor fault diagnosis based on learning. *IEEE Transactions on Instrumentation and Measurement*, (99), 2018.

[32] Ferhat Çira, Müslüm Arkan, and Bilal Gümüş. A new approach to detect stator fault in permanent magnet synchronous motors. In *Diagnostics for Electrical*

Machines, Power Electronics and Drives (SDEMPED), 2015 IEEE 10th International Symposium on, pages 316–321. IEEE, 2015.

[33] Seyed Saeid Moosavi, A Djerdir, Y Aït-Amirat, and DA Kkuburi. Artificial neural networks based fault detection in 3-phase pmsm traction motor. In *Electrical Machines (ICEM), 2012 XXth International Conference on*, pages 1579–1585. IEEE, 2012.

[34] Mikhail Tsypkin. Induction motor condition monitoring: Vibration analysis technique—diagnosis of electromagnetic anomalies. In *AUTOTESTCON, 2017 IEEE*, pages 1–7. IEEE, 2017.

[35] JR Cameron, WT Thomson, and AB Dow. Vibration and current monitoring for detecting airgap eccentricity in large induction motors. In *IEE Proceedings B (Electric Power Applications)*, volume 133, pages 155–163. IET, 1986.

[36] Fabio Immovilli, Alberto Bellini, Riccardo Rubini, and Carla Tassoni. Diagnosis of bearing faults in induction machines by vibration or current signals: A critical comparison. *IEEE Transactions on Industry Applications*, 46(4):1350–1359, 2010.

[37] Mi-Ching Tsai, Shao-Kai Lin, and Sheng-He Wang. Condition monitoring of bldc motor drive systems by hilbert huang transform. In *Ecological Vehicles and Renewable Energies (EVER), 2015 Tenth International Conference on*, pages 1–5. IEEE, 2015.

[38] Mariana Iorgulescu, Magdalena Alexandru, and Robert Beloiu. Noise and vibration monitoring for diagnosis of dc motor's faults. In *Optimization of Electrical and Electronic Equipment (OPTIM), 2012 13th International Conference on*, pages 724–729. IEEE, 2012.

[39] Yoichi Hori, Hideyuki Sawada, and Yeonghan Chun. Slow resonance ratio control for vibration suppression and disturbance rejection in torsional system. *IEEE Transactions on Industrial Electronics*, 46(1):162–168, 1999.

[40] Yuma Yazaki and Hiroshi Fujimoto. Vibration suppression control for two-inertia system using reference governor. In *Advanced Motion Control (AMC), 2018 IEEE 15th International Workshop on*, pages 503–508. IEEE, 2018.

[41] Satomi Hattori, Muneaki Ishida, and Takamasa Hori. Vibration suppression control method for pmsm utilizing repetitive control with auto-tuning function and fourier transform. In *Industrial Electronics Society, 2001. IECON'01. The 27th Annual Conference of the IEEE*, volume 3, pages 1673–1679. IEEE, 2001.

[42] Kenji Kawai, Tadanao Zanma, and Muneaki Ishida. Simultaneous vibration suppression control of pmsm using repetitive control with fourier series. In *Industrial Technology, 2006. ICIT 2006. IEEE International Conference on*, pages 854–859. IEEE, 2006.

[43] Claude Elwood Shannon. Communication in the presence of noise. *Proceedings of the IRE*, 37(1):10–21, 1949.

[44] Kx124-1051 acceleromenter datasheet. `http://kionixfs.kionix.com/en/datasheet/KX124-1051-Specifications-Rev-2.0.pdf`. 10 July 2018.

[45] Kxtc9-2050 acceleromenter datasheet. `http://kionixfs.kionix.com/en/datasheet/KXTC9-2050%20Specifications%20Rev%202.pdf`. 10 July 2018.

[46] María Martínez Gómez. Permanent magnet synchronous machine rotor vibration measurement system. 2017.

[47] ZQ Zhu, S Ruangsinchaiwanich, and David Howe. Synthesis of cogging-torque waveform from analysis of a single stator slot. *IEEE transactions on industry applications*, 42(3):650–657, 2006.

[48] ZQ Zhu and David Howe. Analytical prediction of the cogging torque in radial-field permanent magnet brushless motors. *IEEE transactions on magnetics*, 28(2):1371–1374, 1992.